Gold Nanoparticles: Enhancing the Sensitivity of Clinical Diagnostic Tests

Free Article Collection eBook

The current COVID-19 pandemic has brought much attention to the medical utility of rapid diagnostic test (RDTs). Although these assays are easy to use and provide fast diagnostic results at the point-of-care, one of the main limitations in their development has been the prevalence of false-positive and false-negative results. To improve their sensitivity, gold nanoparticle probes have been incorporated into the design of RDTs. Gold nanoparticles are highly regarded for their optoelectronic properties, biocompatibility, stability, and their ability to be synthesized into various shapes.

Taken together, these features can be utilized in various combinations to optimize the sensitivity and accuracy of clinical diagnostics. Our article collection “Gold Nanoparticles: Enhancing the Sensitivity of Clinical Diagnostic Tests” highlights several applications where gold nanoparticles were used to improve clinical biomarker or disease detection.

Through this research article collection, we hope to educate scientists on how gold nanoparticles can be used to enhance the sensitivity of clinical diagnostic tests.

Download here

nanoComposix | FORTIS LIFE SCIENCES

WIREs Wiley Interdisciplinary Reviews

ADVANCED MATERIALS
www.advmat.de

Advances in High-Performance Autonomous Energy and Self-Powered Sensing Textiles with Novel 3D Fabric Structures

*Kai Dong, Xiao Peng, Renwei Cheng, Chuan Ning, Yang Jiang, Yihan Zhang, and Zhong Lin Wang**

The seamless integration of emerging triboelectric nanogenerator (TENG) technology with traditional wearable textile materials has given birth to the next-generation smart textiles, i.e., textile TENGs, which will play a vital role in the era of Internet of Things and artificial intelligences. However, low output power and inferior sensing ability have largely limited the development of textile TENGs. Among various approaches to improve the output and sensing performance, such as material modification, structural design, and environmental management, a 3D fabric structural scheme is a facile, efficient, controllable, and scalable strategy to increase the effective contact area for contact electrification of textile TENGs without cumbersome material processing and service area restrictions. Herein, the recent advances of the current reported textile TENGs with 3D fabric structures are comprehensively summarized and systematically analyzed in order to clarify their superiorities over 1D fiber and 2D fabric structures in terms of power output and pressure sensing. The forward-looking integration abilities of the 3D fabrics are also discussed at the end. It is believed that the overview and analysis of textile TENGs with distinctive 3D fabric structures will contribute to the development and realization of high-power output micro/nanowearable power sources and high-quality self-powered wearable sensors.

1. Introduction

Textile is one of the basic necessities of people's daily life, which has been accompanied by the development of human civilization for thousands of years. A brief chronology of the evolution of textile materials from ancient times to the present, and then to the future is shown in **Figure 1**, indicating that typical textile materials that can highlight the characteristics of the times have experienced the transformation from natural fiber, artificial/synthetic fiber, reinforced fiber, functional fiber, conductive fiber, and then to smart fiber. Accordingly, the primary purposes or service demands of textile materials have also changed imperceptibly from the aspects of covering, warmth preservation, protection, beauty, security, comfort, health, interaction, and intelligence. On these grounds, it can be found that with the advances of Internet-of-Things and artificial intelligences, textile materials are no longer limited to the traditional functions of protection, warm-keeping, and aesthetic, but should be given more smart or intelligent attributes, such as energy harvesting,[1–3] energy storage,[4,5] autonomous response,[6,7] information interaction,[8,9] data transmission,[10,11] light emitting,[12,13] color changing,[14] shape memory,[15] thermal regulation,[16,17] self-healing,[18a] self-adaption,[19] etc. In addition, considering that human oriented wearable electronics will be highly integrated and miniaturized, completely safe and comfortable, and fully portable in the future, it is also expected to design various functional electronics directly into textile structures, such as fibers, yarns or fabrics.[20,21] At present, a variety of functional attributes have been well integrated with textile materials, mainly including energy,[3,4,12,22] sensing,[8,10,23,24] comfort,[16,25a,26,27] and protection,[19,28–30] which endows this kind of traditional necessity of life with new development vitality (**Figure 2**). In particular, through the seamless combination of electrical functionalities and textile elements, a new type of textiles, namely smart textiles, have been developed, which can perceive, react and adapt to environmental stimuli, including machinery, magnetism, heat, electricity, light, chemistry, biology, and others.[31–35] It can be predicted that the realization of high-performance electrical function and comfortable to wear is the unremitting pursuit goal of the next generation of smart textiles.

It is noteworthy that the effective operation of most additional functions in smart textiles depends on sustained and stable energy sources. In other words, we need reliable, compact but high-performance electricity supply systems to power emerging

K. Dong, X. Peng, R. Cheng, C. Ning, Y. Jiang, Y. Zhang, Z. L. Wang
Beijing Institute of Nanoenergy and Nanosystems
Chinese Academy of Sciences
Beijing 101400, P. R. China
E-mail: zlwang@binn.cas.cn

K. Dong, X. Peng, R. Cheng, C. Ning, Y. Jiang, Y. Zhang, Z. L. Wang
College of Nanoscience and Technology
University of Chinese Academy of Sciences
Beijing 100049, P. R. China

Z. L. Wang
CUSTech Institute of Technology
Wenzhou, Zhejiang 325024, P. R. China

Z. L. Wang
School of Material Science and Engineering
Georgia Institute of Technology
Atlanta, GA 30332, USA

The ORCID identification number(s) for the author(s) of this article can be found under https://doi.org/10.1002/adma.202109355.

DOI: 10.1002/adma.202109355

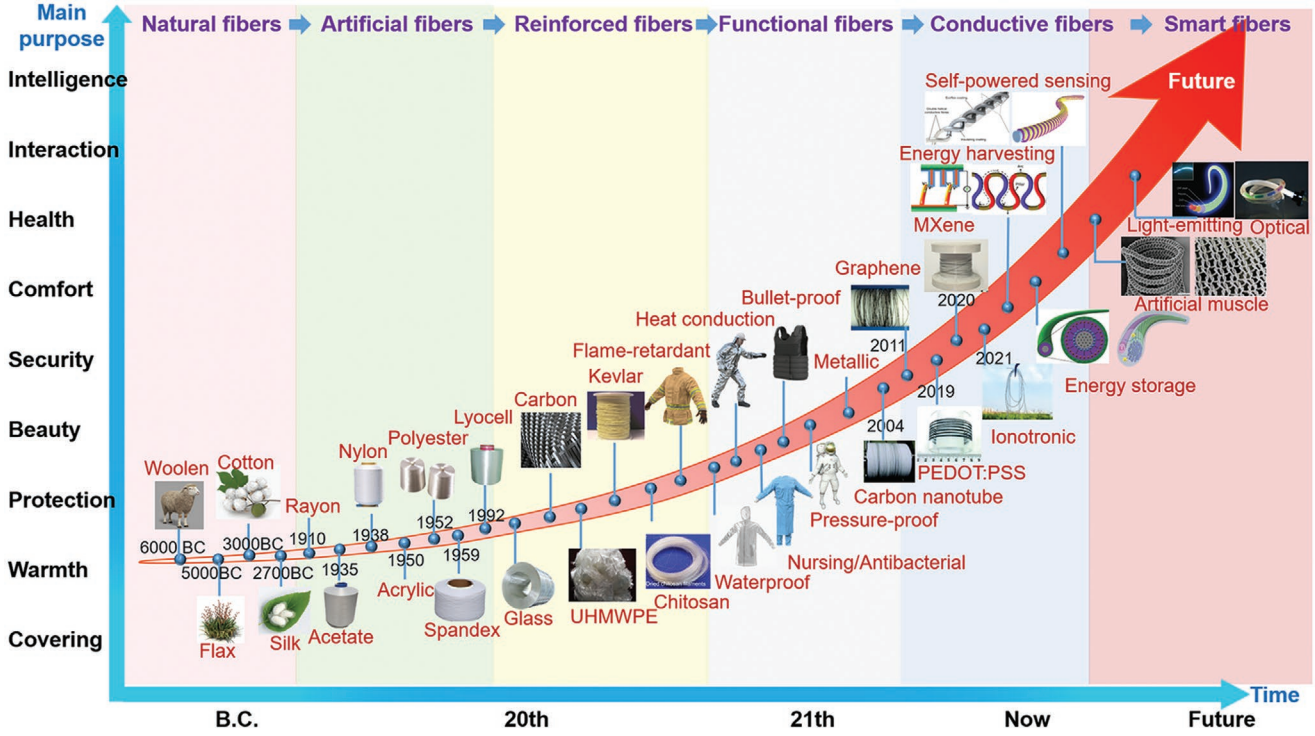

Figure 1. A brief chronology of the evolution of textile materials in the process of human civilization. The abscissa represents the time scale from B.C. to the future, and the ordinate reflects the change of textile materials in terms of the primary purposes and service demands. Representative fiber material types at different stages are highlighted with different background colors and arranged in chronological order, including natural fibers (pink), artificial fibers (green), reinforced fibers (yellow), functional fibers (gray), conductive fibers (blue), and smart fibers (red). It is worth noting that the above arrangement is not strictly in chronological order, but follows the general development law of fiber materials. Images permissions: Kevlar fibers. Reproduced with permission.[184] Copyright 2019, American Chemical Society. Chitosan fibers. Reproduced with permission.[185] Copyright 2021, Wiley-VCH. Carbon nanotube fibers. Reproduced with permission.[186] Copyright 2004, American Association for the Advancement of Science (AAAS). Graphene fibers. Reproduced with permission.[187] Copyright 2011, Springer Nature. PEDOT: PSS fibers. Reproduced with permission.[188] Copyright 2019, The Royal Society of Chemistry. MXene fibers. Reproduced under the terms of the CC-BY Creative Commons Attribution 4.0 International license (https://creativecommons.org/licenses/by/4.0).[189] Copyright 2020, The Authors, published by Springer Nature. Ionotronic fibers. Reproduced with permission.[190] Copyright 2021, Wiley-VCH. Energy harvesting. Left: Reproduced with permission.[191] Copyright 2008, Springer Nature. Right: Reproduced under the terms of the CC-BY Creative Commons Attribution 4.0 International license (https://creativecommons.org/licenses/by/4.0).[192] Copyright 2020, The Authors, published by Springer Nature. Energy storage. Left: Reproduced with permission.[193] Copyright 2013, Wiley-VCH. Right: Reproduced with permission.[194] Copyright 2014, Wiley-VCH. Self-powered sensing. Left: Reproduced with permission.[195] Copyright 2021, The Authors, published by Springer Nature. Right: Reproduced with permission.[18b] Copyright 2022, American Chemical Society. Artificial muscle. Left: Reproduced with permission.[196] Copyright 2019, The Authors, published by AAAS. Right: Reproduced with permission.[197] Copyright 2016, The Authors, published by National Academy of Sciences, USA. Light-emitting. Reproduced with permission.[198] Copyright 2015, Springer Nature. Optical fibers. Reproduced with permission.[199] Copyright 2020, The Authors, published by AAAS. In this figure, UHMWPE represents ultrahigh-molecular-weight polyethylene.

multifaceted on-body electronic devices. Currently, textile-based electrochemical energy storage devices, including fiber-shaped or fabric-like supercapacitors[36,37] and batteries[38,39] have been widely used to provide the required electricity for wearable electronics.[40–43] However, due to their inherent deficiencies, such as limited storage capacity, frequent charging times, calculable service life, potential safety risks, expensive recovery costs, and serious environmental hazards, it is difficult to fundamentally meet the sustainable power supply of numerous wearable electronics and distributed sensor networks.[1,5,44] Alternatively, a feasible solution for powering wearable electronics without additional power input is to directly harvest energy from the surrounding environment and effectively convert it into electricity or electrical signals. As we all know, there are a variety of renewable and green energy forms in our physical world, such as solar energy, thermal energy, mechanical energy, chemical energy, and biological energy.[45–47] Although solar, thermal and biological energies have been effectively collected by solar cells,[48,49] thermoelectric generators,[50,51] and biofuel cells[52,53] respectively, they are too dependent on external factors, such as outdoor sunlight, temperature gradient, and reactive enzymes, making it difficult for them to be used effectively on a large scale. A brief comparison of these renewable energy harvesting forms is further summarized in **Table 1**, from which their respective characteristics, merits and limitations can be easily found. In particular, mechanical energy, especially human movement, is a ubiquitous and widely distributed form of energy, which has always been ignored or wasted for a long time due to its out-of-order form, low energy density, low motion frequency, and low utilization rate. As an emerging mechanical energy harvesting technology, triboelectric nanogenerator (TENG) originated from Maxwell's displacement current can convert randomly

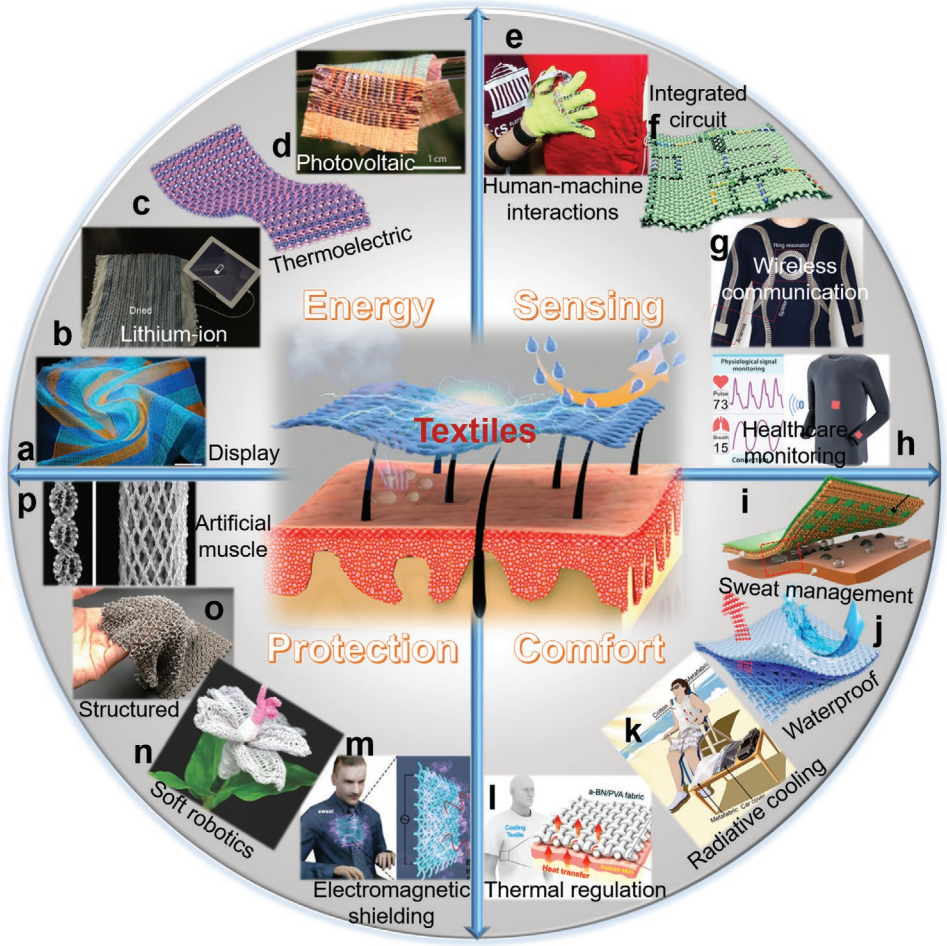

Figure 2. Schematic view of textiles that can be integrated with versatile functional attributes, such as energy, sensing, comfort, protection, and so on. a) Large-area display textiles. b) Woven lithium-ion fiber batteries. c) Scalable thermoelectric fibers for multifunctional textile electronics. d) Hybrid power textile for simultaneously harvesting solar and mechanical energy. e) Body network human–environment interactions with conformal tactile textiles. f) Nonprinted integrated-circuit textile. g) Wireless body sensor networks based on metamaterial textiles. h) Machine-knitted sensor array textile for precise epidermal physiological signal monitoring. i) Skin-like fabric for personal moisture management. j) Water-resistant and highly breathable textiles. k) Hierarchical-morphology metafabric for scalable passive daytime radiative cooling. l) 3D printed thermal regulation textiles. m) Flexible and multifunctional silk textiles for electromagnetic interference shielding. n) Loop-linked soft morphing flower. o) Structured fabrics with tunable mechanical properties. p) Artificial muscles from fishing line and sewing thread. a) Reproduced with permission.[12] Copyright 2021, The Authors, published by Springer Nature. b) Reproduced with permission.[4] Copyright 2021, The Authors, published by Springer Nature. c) Reproduced under the terms of the CC-BY Creative Commons Attribution 4.0 International license (https://creativecommons.org/licenses/by/4.0).[3] Copyright 2020, The Authors, published by Springer Nature. d) Reproduced with permission.[22] Copyright 2016, Springer Nature. e) Reproduced with permission.[8] Copyright 2021, The Authors, published by Springer Nature. f) Reproduced under the terms of the CC-BY Creative Commons Attribution 4.0 International license (https://creativecommons.org/licenses/by/4.0).[10] Copyright 2021, The Authors, published by Springer Nature. g) Reproduced with permission.[23] Copyright 2018, The Authors, published by Springer Nature. h) Reproduced with permission.[24] Copyright 2020, The Authors, published by AAAS. Reprinted/adapted from ref. [24]. © The Authors, some rights reserved; exclusive licensee American Association for the Advancement of Science. Distributed under a Creative Commons Attribution NonCommercial License 4.0 (CC BY-NC) http://creativecommons.org/licenses/by-nc/4.0/. i) Reproduced under the terms of the CC-BY Creative Commons Attribution 4.0 International license (https://creativecommons.org/licenses/by/4.0).[25b] Copyright 2021, The Authors, published by Springer Nature. j) Reproduced with permission.[26] Copyright 2020, American Chemical Society. k) Reproduced with permission.[16] Copyright 2021, The Authors, published by AAAS. l) Reproduced with permission.[27] Copyright 2017, American Chemical Society. m) Reproduced with permission.[28] Copyright 2019, Wiley-VCH. n) Reproduced with permission.[29] Copyright 2017, Wiley-VCH. o) Reproduced with permission.[19] Copyright 2021, The Authors, published by Springer Nature. p) Reproduced with permission.[30] Copyright 2014, AAAS.

distributed, irregular and wasted low-frequency mechanical energy into electric power based on the coupling effect of contact electrification/triboelectrification and electrostatic induction.[54–57] With the merits of wide availability, low cost of preparation, human/environmental friendly, and diverse material selection, TENGs have wide application prospects, including wearable emergency power sources,[58–61] self-powered sensors,[62–65] personal healthcare systems,[24,66,67] human–machine interactions,[68,69] and artificial intelligence.[70,71] It is fantastic that human daily motion energy will be converted into electricity instead of being wasted when TENGs are placed on the surface of the human body. Compared with other existing

Table 1. Brief comparison of various renewable energy harvesting forms.

Energy sources	Main energy harvesting devices	Merits	Limitations	Maximum power
Solar energy	• Photovolatic solar cells	• High power output • Continuous power • DC output	• Highly dependent on external environment • Low-performance without sunlight	1 mW cm^{-2} Outdoor
Mechanical energy	• Triboelectric nanogenerators	• Less dependent on external environment • High voltage	• Pulsed AC input • Require constant movement • Low current • Sensitive to external pollutants	1 mW cm^{-2} Indoor and outdoor
	• Piezoelectric nanogenerators	• Less dependent on external environment • Unsensitive to surface	• Limited material selections • Low voltage • Pulsed AC input • Require constant movement	0.01 mW cm^{-2} Indoor and outdoor
Thermal energy	• Thermoelectric generators	• Continuous power • Unsensitive to surface • DC output	• Low voltage • Limited material selections • Complex structure • Depend on temperature gradient	0.001 mW cm^{-2} Indoor and outdoor
	• Pyroelectric nanogenerators	• Spatially uniform temperature • Independ of temperature gradient	• Pulsed AC input • Limited material selection • Depend on temperature fluctuation	0.001 mW cm^{-2} Indoor and outdoor
Biomass energy	• Biofuel cells • Microbial fuel cells	• Continuous power • Less dependent on external environment • DC output	• Limited fuel availability • Low voltage • High cost • Sensitive to external pollutants	1 mW cm^{-2} Indoor and outdoor

forms, such as carrying, attaching, wrapping and embedding, textiles can be seamlessly combined with electrical functions without extra burden and aesthetic sacrifice, thus providing versatile design carriers and broad service platforms for TENGs. To this end, a new type of smart textiles with mechanical energies harvesting ability and excellent wearing comfort, namely TENG-based smart textiles, are emerging and developing rapidly, which opens up a new research direction for smart textiles.[72,73]

Wearable emergency power sources and self-powered pressure sensors are the two main application fields of the burgeoning TENG-based smart textiles, as illustrated in **Figure 3**. Although large numbers of research works have been done in these two aspects, their scalable development and practical application are still restricted by two bottlenecks, i.e., low power output and inferior sensing ability. Although there are several strategies to improve the power density and sensing sensitivity of TENGs, such as surface/interface modification,[74,75] material selection/optimization,[76,77] structural design/analysis,[78,79] charge shuttling/pumping,[80,81] power management,[82,83] and environmental control,[84] most of them rely on professional instruments, complex preparation technology, cumbersome processing process, and even special air conditions, which are difficult to achieve low-cost, large-scale and high-quality preparation, and even more difficult to effectively apply to textiles. In particular, for fabrics interwoven by fibers from different orientations, it is possible to make full use of internal space structure to increase the effective contact area between the pairs of triboelectrification layers. Compared with 1D fiber and 2D fabric, the 3D fabric not only increases the number of layers of fiber arrangement in the in-plane direction, but also introduces bonding fibers in the thickness (out-of-plane) direction, thus increasing the structural integrity and dimensional stability. Multilayered fiber distribution is able to create more contact–separation space that can effectively improve the power output density of textile TENGs. In addition, 3D fabric structures can also realize the gradual contact response between fibers from point to line and then to surface, which can improve the sensitivity and response speed of pressure sensing. Moreover, although highly sensitive self-powered sensing fabrics have been widely reported, few research can achieve simultaneous response to static and dynamic pressure due to the limitation of conventional 2D fabric structures. 3D fabric structures provide a new combination design scheme for a wide range of pressure response. Based on these merits, 3D fabric structures are particularly suitable for the design and fabrication of high-performance TENG-based smart textiles.

Figure 3. Schematic illustration of on-body textile-based TENGs as micro/nanopower sources and self-powered active sensors.

In this review, the basic operation modes of TENGs and their corresponding service occasions, as well as their electrical generation and transfer mechanisms are briefly summarized. In addition, the potential feasible approaches for improving the power output and self-powered sensing performance of TENGs are also analyzed. Furthermore, the state of the arts of TENG-based smart textiles with advanced 3D fabric structures, including 3D woven, 3D knitted, 3D braided, 3D nonwoven, 3D printing, and 3D multilayer stacking, are comprehensively overviewed and systematically investigated. On the basis of the literature research and elaborated discussion, the advantages of 3D fabric structures in improving power output density and pressure sensing sensitivity of textile TENGs compared with 1D fibers and 2D fabrics are revealed. In the end, two main forward-looking and prospective research directions of smart textiles with advanced 3D fabric structures are proposed, including efficient acquisition and synchronous storage of multiple energy forms, and real-time response and self-powered sensing of multimode pressure signals. It is hoped that this review will make a comprehensive understanding of textile TENGs and provide a novel 3D fabric structure design idea for the research and application of high-performance TENG-based smart textiles.

2. Advanced 3D Fabric Structures

A prominent feature of textiles is that they have a variety of structural forms, which can be roughly divided into 1D fibers or yarns, 2D fabrics, and 3D fabrics from the perspective of structural dimensions. 1D fibers or yarns are the basic components of fabrics, which have the features of high aspect ratio, high specific surface area, continuous conductive channel, multilevel hierarchical distribution, and so on.[85–87] 1D fibers or yarns can be further processed into 2D or 3D fabrics through various textile forming methods or processing techniques. 2D fabrics are the most common and widely used textile structures due to their mature fabrication techniques, unlimited in-plane sizes, and broad application ranges. However, due to the lack of fiber interlacing in thickness direction, traditional 2D fabrics are troubled by their low out-of-plane mechanical properties. In order to overcome this shortcoming, the binding reinforcing yarn is introduced into the thickness direction, thus forming 3D fabric structures, which is an industrial process for producing volumetric material through organized multiaxial interlacing of fibers. 3D fabrics are a kind of textile constructions that have at least three fiber systems with different orientations. In other words, fibers are intertwined, interlaced or intermeshed in the longitudinal (*X*), transverse (*Y*), and thickness (*Z*) directions. Therefore, 3D fabric structures are usually endowed with several distinct properties, such as structural integrity, dimension stability, spatial interlacing network, and out-of-plane enhancement effect, which have great application prospects in the fields of composite material manufacturing, architectural engineering, furnishing decorations, sport apparatus, medical instruments, and more.[1,88–91] From the perspective of manufacturing techniques and basic structural features, 3D fabric structures can be divided into 3D weaving, 3D knitting, 3D braiding, 3D nonwoven, 3D printing, 3D multilayer stacking, and etc. Below, we will briefly introduce their respective typical representatives, structural characteristics, and prominent merits (**Table 2**).

3D woven fabrics contain a group of fibers running through the whole thickness direction that can bond the in-plane layers at varying angles to form a whole, which are mainly divided into 3D orthogonal woven fabric (3DOW) and 3D angle-interlock woven fabric (3DAW).[92] 3DOW consists of three groups of mutually perpendicular yarns, in which *Z*-yarns interconnect all individual warp- and weft-directional yarns to each other, thus solidifying the fabric, as shown in **Figure 4**a. 3DAW contains at least two sets of yarns, which are divided into two groups, i.e., 3D layer-to-layer angle interlock fabric (3DLAW, Figure 4b) and 3D through-the-thickness angle-interlock fabric (3DTAW, Figure 4c). In 3DLAW, warp yarn travels from one layer to the adjacent layer and back, while in 3DTAW, warp yarn travels from one surface of the 3D fabric to the other, thus holding all the layers together. 3D knitting is composed of yarn loops connected to each other and adjacent rows and columns by various techniques.[93] Among various 3D knitting fabrics, 3D knitted spacer fabric is a sandwich structure consisting of two separate outer knitted substrates that are joined together or kept apart by spacer yarns, which are oriented in the third dimension (Figure 4d).[94] 3D braided fabrics are formed by interlacing three or more yarns to form an integral structure, which have high-dimensional stability and structural integrity.[95] An important characteristic of 3D braided fabrics is their ability to form a variety of complex shapes, such as rectangular

Table 2. Basic characteristics and classifications of 3D fabric structures.

Structures	Typical representatives	Characteristics	Merits
3D woven	Orthogonal, angle-interlock	*Z*-yarns binding through the thickness direction	High production rates, high-dimensional stability
3D knitted	Spacer weft/warp-knitted	Low fiber volume fraction, Looped structure	High stretchability, extensibility and drapeability, huge flexibility and stability
3D braided	Four/five-directional, rectangular/tubular shape	Infinite length while finite cross section	High shape adaptability, highly automated, readily available
3D nonwoven	Web, sheet, felt, electrospinning	Consisting of millions of individual fibers	Large surface area to mass, high pore volume, tight pore size, and high density
3D printing	Fused deposition modeling, direct ink writing	Incorporating multimaterial components to produce complex structures	Rapid prototyping, facile fabrication, versatile design, high reproducibility
3D multilayer stacking	Melt	Multiple 2D fabrics stacked along the thickness direction	Easy to scale, simple to fabricate

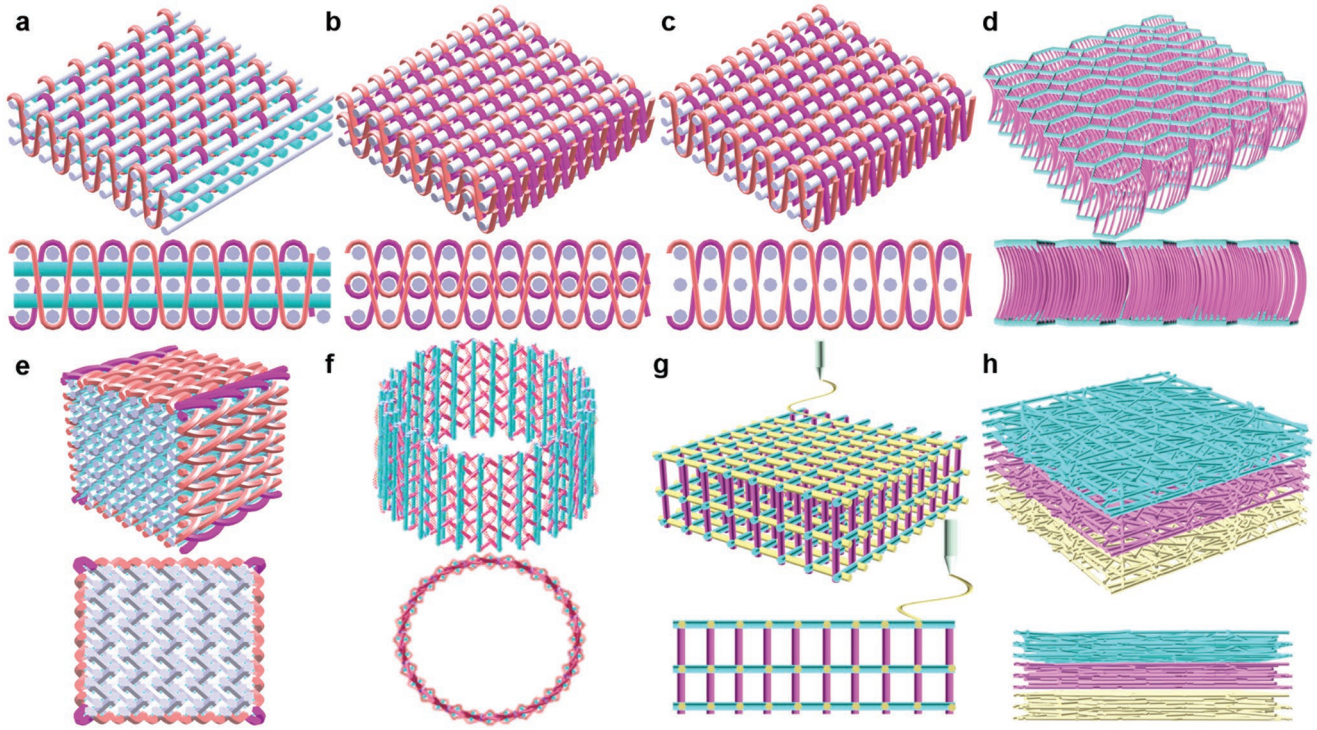

Figure 4. Classifications of 3D fabric structures, including: a–c) 3D woven structures, such as 3D orthogonal woven (a), 3D layer-to-layer angle-interlock woven (b), and 3D through-to-thickness angle-interlock woven (c), d) 3D warp spacer knitted, e,f) 3D braided structures, such as 3D five-directional rectangle braided (e) and 3D five-directional circular braided (f), g) 3D printing fabric structures, and h) 3D multilayered nonwoven structures.

shape (Figure 4e) and tubular fashion (Figure 4f). 3D nonwoven nanofibrous scaffolds consist of millions of individual fibers, in which fibers form a network structure and are finally bonded together by various techniques, such as bonding, stitching, felting, and thermal fusion (Figure 4g).[96,97] In 3D nonwovens, fibers are assembled into a planar structure and interlocked to form porous sheets with a certain degree of flexibility. Among various techniques, electrospinning is a facile and broadly used nonwoven manufacturing technique, which can fabricate micro/nanoscale fibers in a continuous process.[98] 3D nonwovens are most commonly used for a wide range of filtration applications, because they have large surface area to mass ratio, high pore volume, tight pore size, and high density. Emerging 3D printing technology is a process whereby parts or components are directly built from a solid model using a heat source and filler material, which includes fusion deposition modeling, direct writing, selective laser sintering, stereo lithography, and so on.[99] In addition, 3D printing is also a possible future application for mass customization of textile products, which can incorporate multimaterial components to produce complex textile structures (Figure 4h).[100] 3D multilayer stacking is one of the simplest ways to fabricate 3D textiles by stacking multiple 2D fabrics along the thickness direction, which is easy to scale on the basis of preparation technique of 2D fabrics.[101] Supporting structures are often built between layers by means of needing, suturing or others in order to enhance the interfacial adhesion. Of course, in addition to the listed above, there are also some other ways to fabricate 3D fabrics, which need to be further explored. It can be found that each of the above-mentioned manufacturing technologies for 3D fabrics has its own advantages and disadvantages in terms of specific performance, and can be selected based on the end-use.

3. Working Modes

Since the first reported of TENG in 2012,[102] significant efforts have been devoted to converting mechanical energy into electricity by various modes of TENGs. According to circuit connection methods and applied loading directions, TENGs can be divided into four basic working modes, namely vertical contact–separation (CS) modes, lateral sliding (LS) mode, single-electrode (SE) mode, and freestanding triboelectric-layer (FT) mode (**Figure 5**).[103] The vertical CS mode utilizes the polarization in a vertical direction and relies on the vertical movement of two perpendicular triboelectric layers. Due to the advantages of high output voltage, the vertical CS mode has been extensively applied to harvest pressing,[104] impacting,[105] bending, shaking and vibration energies.[106] The LS mode depends on the polarization in the lateral direction, due to the lateral sliding between the two contact objects. It would be used for rotational and air/water flow energy harvesting because of high frequency, continuous and high electricity output, which has also been successfully applied in tactile sensing,[107] barcode recognition,[108] and virtual and augmented reality.[109] However, the stability of long-time working and robustness of friction surface is a critical question in practical application. The SE mode with only one electrode is designed to harvest

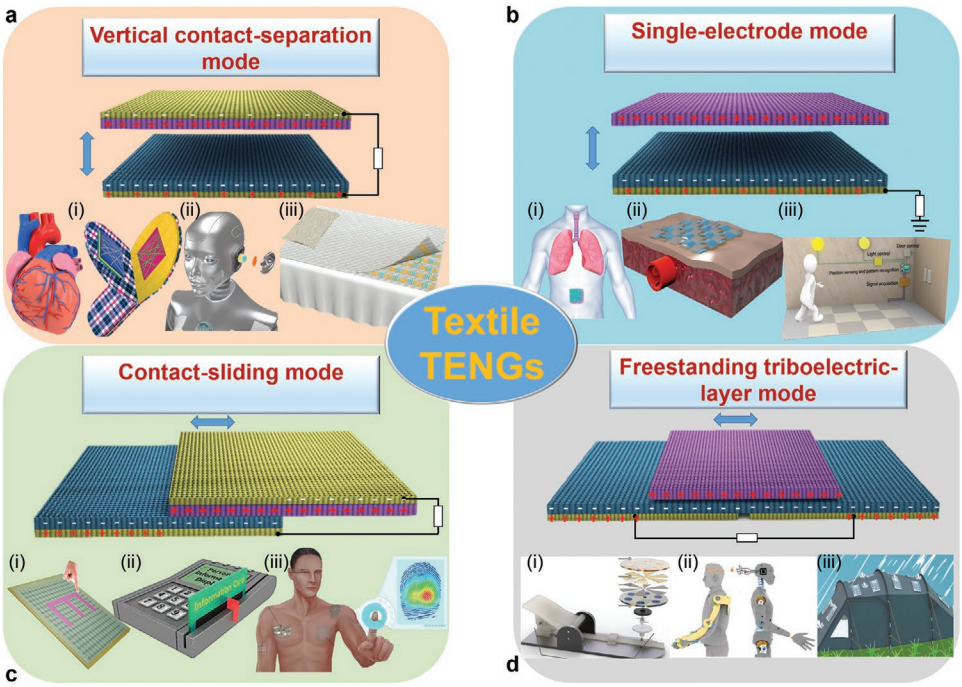

Figure 5. Four fundamental operational modes of textile-based TENGs, including: a) vertical contact–separation mode, b) single-electrode mode, c) in-plane contact-sliding mode, and d) freestanding triboelectric-layer mode. a) i) Reproduced with permission.[105] Copyright 2012, Elsevier. ii) Reproduced with permission.[106] Copyright 2018, The Authors, published by AAAS. iii) Reproduced with permission.[104] Copyright 2017, Wiley-VCH. b) i) Reproduced with permission.[112] Copyright 2021, Wiley-VCH. ii) Reproduced with permission.[111] Copyright 2021, Elsevier. iii) Reproduced under the terms of the CC-BY Creative Commons Attribution 4.0 International license (https://creativecommons.org/licenses/by/4.0).[70] Copyright 2020, The Authors, published by Springer Nature. c) i) Reproduced with permission.[107] Copyright 2021, Wiley-VCH. ii) Reproduced with permission.[108] Copyright 2018, Elsevier. iii) Reproduced with permission.[109] Copyright 2021, Wiley-VCH. d) i) Reproduced under the terms of the CC-BY Creative Commons Attribution 4.0 International license (https://creativecommons.org/licenses/by/4.0).[114] Copyright 2020, The Authors, published by John Wiley & Sons Australia, Ltd on behalf of UESTC. ii) Reproduced under the terms of the CC-BY Creative Commons Attribution 4.0 International license (https://creativecommons.org/licenses/by/4.0).[115] Copyright 2021, The Authors, published by Springer Nature. iii) Reproduced with permission.[116] Copyright 2020, American Chemical Society.

energy from a freely moving object without attaching an electric conductor, which is suitable for fabricating sliding/typing/touch screen. Owing to simple fabrication, easy to carry, and versatility in energy harvesting, the SE mode has been developed in wearable electronics,[110] fitness monitoring,[111,112] soft robotics,[113] and human–machine interface.[70] The FT mode comprises a triboelectric layer and two stationary symmetrical electrodes. It is designed for rotational and vibration energy harvesting in virtue of high energy conversion efficiency, which has been used for noncontact free-rotating sensor,[114] multiple degree of freedom sensor,[115] and raindrop kinetic energy collection.[116] The four basic working modes have been widely demonstrated, each of which has different design methods to accommodate the corresponding mechanical triggering conditions. Enabled by different structural characteristics, the four working modes of TENGs have their own suitable application scenarios, as summarized in **Table 3**.

Table 3. Comparison of the four working modes of TENGs.

Modes	Main application occasions
Contact–separation (CS)	Pressing, impacting, bending, sharking, vibration
Lateral sliding (LS)	Rotational and air/water flow energy harvesting
Single electrode (SE)	Sliding/typing/toughing screen
Freestanding triboelectric-layer (FT)	Rotational and vibration energy harvesting

4. Theory of Textile TENGs from Expanded Maxwell's Equations

Maxwell's equation, as one of the ten most important equations for physics, is the foundation of modern wireless communication, photonics and optical communication.[57] One of the greatest creative ideas from the equations is the introduction of a displacement current in order to satisfy the conservation law of charges. Recently, to account for the contribution made by the contact electrification-induced electrostatic charges during the mechanical agitation for power generation, the expression of displacement current has been expanded,[56,117] in which a new term $\mathbf{P}_s$ in $\mathbf{D}$ is first introduced for deriving the output power of NGs.[118] The electric displacement vector $\mathbf{D}$ can be described as

$$\mathbf{D} = \varepsilon_0 \mathbf{E} + \mathbf{P} + \mathbf{P}_s \quad (1)$$

where $\mathbf{P}_s$ is the polarization caused by the electrostatic surface charges on medium passing through the space due to mechanical triggering, which is different from the electric field-induced

polarization of the medium **P**. By redefining a new vector **D′**, where $\mathbf{D}' = \varepsilon_0\mathbf{E} + \mathbf{P}$, the expanded Maxwell's equations can be expressed as

$$\nabla\cdot\mathbf{D}' = \rho' \text{(Gauss's law)} \tag{2}$$

$$\nabla\cdot\mathbf{B} = 0 \text{(Gauss's law for magnetism)} \tag{3}$$

$$\nabla\times\mathbf{E} = -\frac{\partial\mathbf{B}}{\partial t} \text{(Faraday's law)} \tag{4}$$

$$\nabla\times\mathbf{H} = \mathbf{J}' + \frac{\partial\mathbf{D}'}{\partial t} \quad \text{(Ampere's circuital law with Maxwell's addition)} \tag{5}$$

where the electric field **E**, the magnetic field **B**, magnetizing field **H**, the free electric charge density ρ', the free electric current density J′, displacement field **D**. If the medium makes a translational motion of a rigid body in space, in which the translation velocity is *v*, the volume charge density and the density of current density can be redefined as

$$\rho' = \rho - \nabla\cdot\mathbf{P_s} \tag{6}$$

$$\mathbf{J}' = \mathbf{J} + \rho v + \frac{\partial\mathbf{P_s}}{\partial t} \tag{7}$$

Based on the charge conversion and continuation equation

$$\nabla\cdot\mathbf{J}' + \frac{\partial\rho'}{\partial t} = 0 \tag{8}$$

With the conduction current **J**, the total displacement current is

$$\mathbf{J_D} = \frac{\partial\mathbf{D}'}{\partial t} + \frac{\partial\mathbf{P_s}}{\partial t} \tag{9}$$

where $\frac{\partial\mathbf{D}'}{\partial t}$ represents the displacement current due to the time variation of electric field, and the term $\frac{\partial\mathbf{P_s}}{\partial t}$ is the current due to the change in media boundary.[56,57] These equations are the cornerstones of the electricity generation of textile TENGs.

5. Electricity Generation and Transport Mechanisms

Fiber refers to a kind of material with large aspect ratio, small diameter, and flexibility to some extent, which can be easily assembled into yarn by fiber clustering methods, such as twisting, wrapping, braiding, spinning, weaving and others. The integrated yarn has a hierarchical configuration and uneven surface, which makes its interface with external bonding materials extremely complex. In addition, there are many micro- or nanostructural defects on the surface of fibers or yarns, including convex, crack, hairiness, concave, crevice, and more, as exhibited in **Figure 6**a. Therefore, it is rather difficult to fully investigate the contact electrification behavior of fiber-based TENGs, which has also never been done before. However, the basic electricity generation process of planar TENGs that is proposed with the first invention of TENGs[102] can help us better analyze the charge generation and transport process of fiber-based TENGs. As shown in the Figure 6b, an alternating current signal corresponds to a contact–separation period, which can be explained based on the coupling effect of contact electrification/triboelectrification and electrostatic induction. In the initial state, a separation distance between the two kinds of active triboelectric materials is maintained due to the difference of micro- and nanostructures. Once the two kinds of active triboelectric materials are in contact with each other under the action of external force, electrons will be injected from one into the other, resulting in the induction of triboelectric charges on their surface. When the contact surfaces are separated, a potential difference will be established between the two electrodes, which will drive free electrons to flow between them to shield local electric field. And if the two surfaces come into contact again, a potential difference with reversed polarity and current will flow back in the opposite direction, making a complete cycle of electricity generation. In addition, an atomic-scale electron cloud/wave-function overlap model is often proposed to explain the contact electrification induced electricity generation and transport mechanisms of TENGs.[119–121] Interatomic interaction potential can reflect the repulsion and attraction interactions between two atoms. When two atoms form a bond that represents some kind of overlap in electron clouds or wave functions, the equilibrium distance is established. By comparing bond length or interatomic distance with this equilibrium distance, we can judge whether the two atoms are in contact or tend to repel each other, thus judging whether the electron clouds overlap.[57] As shown in Figure 6c, the possible process of electron transfer between two atoms is also explained. In the initial stage (i), before the atomic-scale contact of each other, the electron clouds of the two materials A and B remain separate without overlap. Their electrons are tightly bound in specific orbits in their respective potential wells, which are restricted from escaping freely. When the atoms get close and contact with each other, the electron cloud overlaps between two atoms to form a chemical bond. In this case, the initial single potential well becomes an asymmetric double-well potential, and the energy barrier between them is reduced due to the overlap of strong electron clouds (ii). When they are far away from each other, electrons will flow from A to B, and most of the transferred electrons will stay in B, resulting in contact electrification (iii). In addition, the mechanical contact between the two materials can shorten the distance between the atoms, and cause their electron clouds to overlap strongly in the repulsive region.

6. Approaches to Increasing Power Output and Sensing Ability

The low power output and unsatisfactory sensing ability are always one of the main problems that restrict the large-scale application of TENGs. Various strategies have been tried to improve the performance of TENGs in the two aspects, which can be mainly classified as surface/interface modification, material selection/optimization, structural design, power or circuit management, and environmental control (**Figure 7**). Surface/interface modification is mainly used to increase the

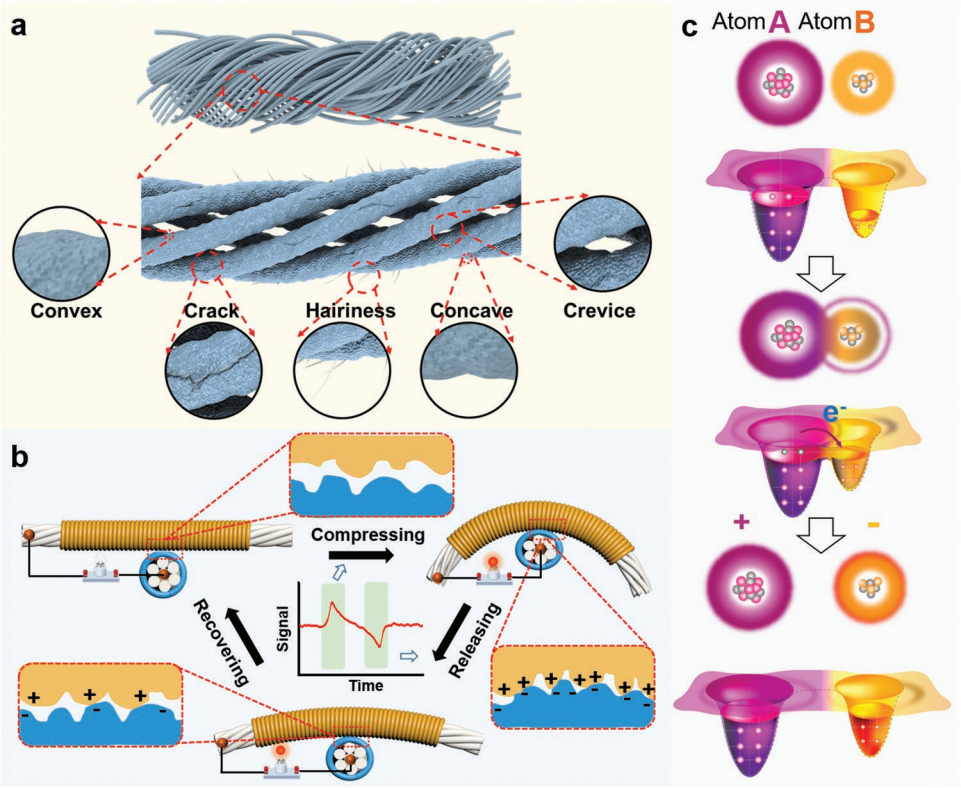

Figure 6. Electricity generation and transfer mechanism of fiber TENGs. a) Typical micro- and nanostructural defects in fibers, including convex, crack, hairiness, concave, and crevice. b) Working principle of fiber TENGs in a complete contact and separation cycle. c) Electron cloud-potential well models, including: i) electron clouds before colliding, ii) electron clouds in colliding, and iii) electron clouds after colliding.

effective contact area of the paired charged surfaces or endow the surfaces with some additional functions. Taking TENGs in vertical CS mode as an example, the charged surface pairs are not completely in contact, which is limited by the material texture and surface inhomogeneities. Some measures have been taken to increase the effective contact area, thus increasing the surface charge, such as manufacturing a linear or cubic or pyramidal polymer pattern arrays on the surface of PDMS,[102] adopting silicone rubber and a rolling liquid to make the inner core which allows soft contact[122] (Figure 7a). Material selection/optimization is also a widely used method to increase the overall power output. Dielectric or surface polarization is a common strategy for increasing surface charge density. Because of the electric hysteresis effect of dielectric polarization, the friction electric field or electrostatic field will cause polarization of ferroelectric materials. At the time of surface polarization balance, ferroelectric materials inside the rest of the dielectric polarization enhances the ability of electronic surface of gain and loss, which in turn enhances the surface polarization, so as to improve the charge density. For example, high-performance triboelectric sensors based on ferroelectric multilayer nanocomposites with alternating layers of poly(vinylidenefluoride-*co*-trifluoroethylene) (PVDF-TrFE) and barium titanate ($BaTiO_3$) nanoparticles are introduced (left side in Figure 7b).[123] In order to keep the triboelectric charges to prevent them from dissipating, charge trapping or storage elements are always mixed into triboelectric materials. For instance, a multifunctional layered TENG is designed, in which a mixed layer of reduced graphene oxide and silver nanoparticles is added between PVDF triboelectric layer and bottom aluminum electrode to trap and block the interfacial charges (right side in Figure 7b).[124] In addition, although the triboelectric series for a wide range of polymers has been quantified to reveal the inherent trend of polymers gaining or losing electrons,[125–127] the triboelectric charge density of polymers can still be changed through adjusting the functional groups with different electron-withdrawing or electron-donating abilities on the surface. As shown in Figure 7c, through the polyamidation reaction, carbon nanotubes (CNTs) and poly(ethylene terephthalate) (PET) are chemically grafted on the surface of polyester fiber, and a kind of textile TENG with enhanced output is obtained.[128] In order to solve the issues of low precision and poor stability of traditional surface modification methods, a new scheme based on helium ion irradiation[129] or nitrogen ion implantation[130] to inject extra electrons or ions is also developed (Figure 7d). In addition, the external charge excitation strategy through charge pump or shuttle is also an effective method to improve the surface triboelectric charge density (Figure 7e).[81] In other cases, considering that the surface charge of two different friction surfaces cannot exceed a certain threshold, the increase of the surface charge density alone is unable to further improve output performance. Under this case, the threshold of power output density can be increased by structural design. For example, a layer of aluminum coated with gold nanoparticles is introduced between the common double-layer CS-TENG, which can increase the output power by over 16 times.[78] In addition, due

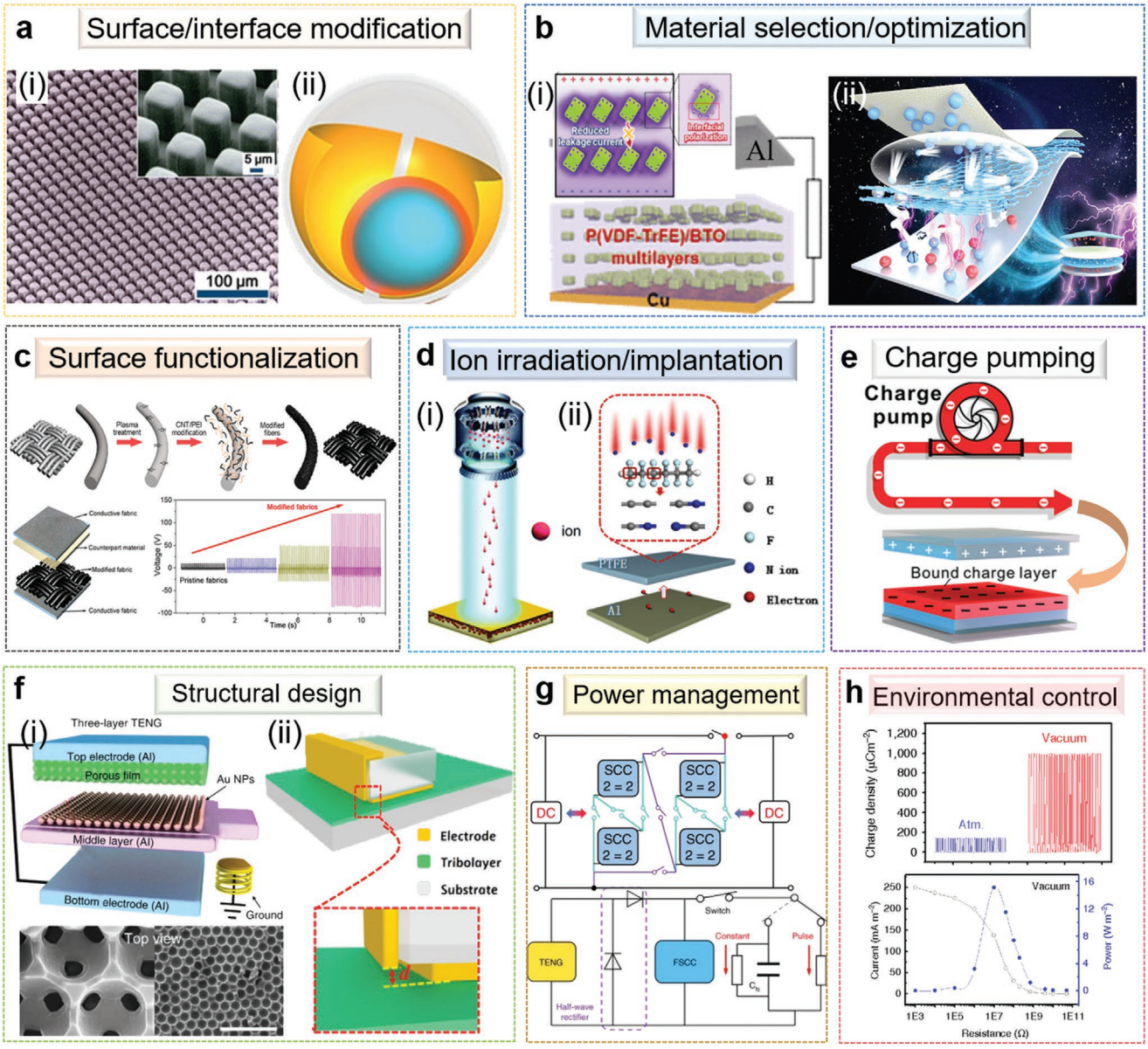

Figure 7. Approaches to improving the power output density of TENGs. a) Surface or interface modification through nanostructures and soft contact. b) Material selection and optimization through ferroelectric polarization. c) Surface functionalization by chemical modification. d) Ion irradiation or implantation by directly injecting ions into polymers. e) Charging pumping/shuttling approach. f) Structural designs via electric double layer effect and electrostatic breakdown effect. g) Power management through switched capacitor convertors. h) Environmental control under vacuum condition. a) i) Reproduced with permission.[102] Copyright 2012, American Chemical Society. ii) Reproduced with permission.[122] Copyright 2019, Elsevier. b) i) Reproduced with permission.[123] Copyright 2020, American Chemical Society. ii) Reproduced with permission.[124] Copyright 2020, Elsevier. c) Reproduced with permission.[128] Copyright 2021, American Chemical Society. d) i) Reproduced with permission.[129] Copyright 2020, The Royal Society of Chemistry. ii) Reproduced with permission.[130] Copyright 2021, Elsevier. e) Reproduced with permission.[81] Copyright 2018, Elsevier. f) i) Reproduced under the terms of the CC-BY Creative Commons Attribution 4.0 International license (https://creativecommons.org/licenses/by/4.0).[78] Copyright 2016, The Authors, published by Springer Nature. ii) Reproduced with permission.[79] Copyright 2019, AAAS. Reprinted/adapted from ref. [79]. © The Authors, some rights reserved; exclusive licensee American Association for the Advancement of Science. Distributed under a Creative Commons Attribution NonCommercial License 4.0 (CC BY-NC) http://creativecommons.org/licenses/by-nc/4.0/. g) Reproduced under the terms of the CC-BY Creative Commons Attribution 4.0 International license (https://creativecommons.org/licenses/by/4.0).[83] Copyright 2020, The Authors, published by Springer Nature. h) Reproduced under the terms of the CC-BY Creative Commons Attribution 4.0 International license (https://creativecommons.org/licenses/by/4.0).[84] Copyright 2017, The Authors, published by Springer Nature.

to high-voltage air breakdown effect, the accumulated surface charges can easily diffuse into the atmosphere and internal frictional layer, leading to charge loss and decrease of surface charge density.[131,132] In order to avoid the negative impact of air breakdown effect, a kind of direct-current TENG (DC-TENG) has been developed, which has the coupling effect of triboelectrification and electrostatic breakdown.[79] By simply adding a breakdown electrode, the DC-TENG can realize DC

electrical output without rectifier bridge, which greatly increases the output power and breaks through the output of traditional TENG limited by electrostatic breakdown (Figure 7f). For example, a highly flexible and wearable fabric DC-TENG with high power output has been developed by simply coating breakdown electrode and friction electrode on the top and bottom side of a polyester-cotton fabric, respectively.[133] By effectively harvesting surface charges from triboelectrification through the conductive plasma channel caused by air breakdown, the DC-TENG can light up 99 bulbs and 1053 LEDs and drive electronic devices directly without rectifying or capacitor charging. Besides the above material and structural methods, attention should also be paid to output management and environmental impact. It is well known that one of the typical characteristics of TENGs is the high output voltage and low output current, which are not suitable for most wearable electronics. Therefore, it is necessary to adjust the electrical output by means of power supply or circuit management to meet the application requirements. Although the traditional transformer can realize the transition from high voltage and low current to low voltage and high current, it needs higher working frequency. However, the switch-capacitor converter has some problems, such as high output impedance and large switching loss. In order to improve the power efficiency, a fractal design switching capacitor converter has been designed, which can achieve over 94% power transmission efficiency (Figure 7g).[83] It is indicated above that air breakdown caused by high-voltage discharge will greatly hinder the improvement of TENGs. Therefore, environmental control such as reducing air pressure can be adopted to reduce the possibility of air breakdown, thus increasing the power output density (Figure 7h).[84] However, although these methods can effectively improve the electromechanical conversion performance of TENGs, it is difficult to apply them to fiber or fabric materials with special structural characteristics, which also urges us to seek new methods to improve the electrical performance of textile TENGs.

7. 3D Fabric TENGs

Because of the structural particularity of textile materials, the above methods that have been developed to improve the performance of TENGs are difficult to be effectively applied to the textile TENGs. Fortunately, through the 3D fabric structures, we turn the disadvantages caused by the special textile structures into the advantages of designing high-performance TENGs. Here, textile-based TENGs with advanced 3D fabric structures including 3D woven, 3D knitted, 3D braided, 3D nonwoven, 3D printing, and 3D multilayer stacking are summarized.

7.1. 3D Woven Structures

Due to the advantages of mechanical robustness and stability, 3D woven structures have been widely used to fabricate high-performance composites. Among all kinds of 3D woven fabrics, 3D orthogonal woven (3DOW) and 3D angle-interlock woven (3DAW) architectures are the most commonly used structures. In 3DOW, there are three directions of yarn systems, i.e., warp yarns in the *X* direction, weft yarns in the *Y* direction, and through-the-thickness binding yarns in the *Z* direction. In particular, *Z*-binding yarns solidify the fabric by interconnecting warp and weft yarns. For instance, a 3DOW TENG is designed for effective biomechanical energy harvesting and active motion signal tracking. As shown in **Figure 8**a, the 3DOW-TENG is composed of three groups of yarns, namely stainless steel/polyester fiber blended yarns as the warp fibers, PDMS-coated energy-harvesting yarns as the weft fibers, and nonconductive cotton yarns as the bonding *Z*-yarns, which are interwoven up and down along the warp yarns over the weft yarns.[134] The maximum output power density of the 3DOW-TENG can achieve 263.36 mW m^{-2}, which is several times higher than that of conventional 2D textile TENGs (Figure 8b). Furthermore, a self-powered dancing blanket is demonstrated to harvest human walking energy and capture human motion signals simultaneously (Figure 8c). Compared with 3DOW, 3DAW is fabricated with two sets of yarns, which obsesses more interspace between yarns and more easily deforms. As presented in Figure 8d, a 3DAW-TENG is developed by silicone rubber coated graphene oxide/cotton composite yarns for improving output performance.[135] Under a pressure of 10 N, the 3DAW obtains the output power of 225 mW m^{-2} (Figure 8e). In virtue of high output performance, the 3DAW-TENG can be used as self-powered sensors, such as carpet signal monitor for energy harvesting and human movement monitoring (Figure 8f). To be compatible with the traditional textile production process, a 3D honeycomb-structured woven fabric (3DHW-TENG) is fabricated of a flame-retardant wrapping yarn by a continuous hollow spindle fancy twister technology (Figure 8g).[136] The 3DHW-TENG can reach the output power of 73.55 μW m^{-1} (Figure 8h). The 3DHW-TENG is designed for smart carpets as a self-powered escape and rescue system, which can achieve precise position locating and reminding the escape route to the survivors (Figure 8i). It is worth noting that although 3D woven fabrics increase the structural complexity, they can easily achieve large-scale and rapid production by properly adjusting the current mature 2D woven fabric preparation process.

7.2. 3D Knitted Structures

Compared to other 3D textile structures, 3D knitted structures are endowed with excellent stretchability, elasticity, and inherent internal spaces so that they can provide larger contact and separation spaces. Therefore, 3D knitting structures have been widely adopted to design 3D fabric TENGs. For example, a 3D double-faced interlocking fabric TENG (3DFIF-TENG) is fabricated by knitting the two system yarns, namely cotton yarns and polyamide (PA, nylon 66) composite yarns.[137] As shown in **Figure** 9a-i, the PA composite yarn is modified by coating Ag electrode and further wrapping silicone rubber. The peak energy output of the 3DFIF-TENG reaches 470 nJ one circle with 200 MΩ external load resistance (Figure 9aii). The 3DFIF-TENG can generate electricity by bending and stretching itself, which can also be used as pressure or weight sensors (Figure 9a-iii). In addition, in order to further increase contact and separation spaces, a fully stretchable 3D rib-knitted fabric TENG (3DRK-TENG) with double-arc shaped structure is fabricated.[138] As shown in Figure 9b-i, the 3DRK-TENG is composed of Ag-coated conductive fabric as the middle layer and two Ag coated PTFE fabrics as the two outer layers. The 3DRK-TENG shows a high

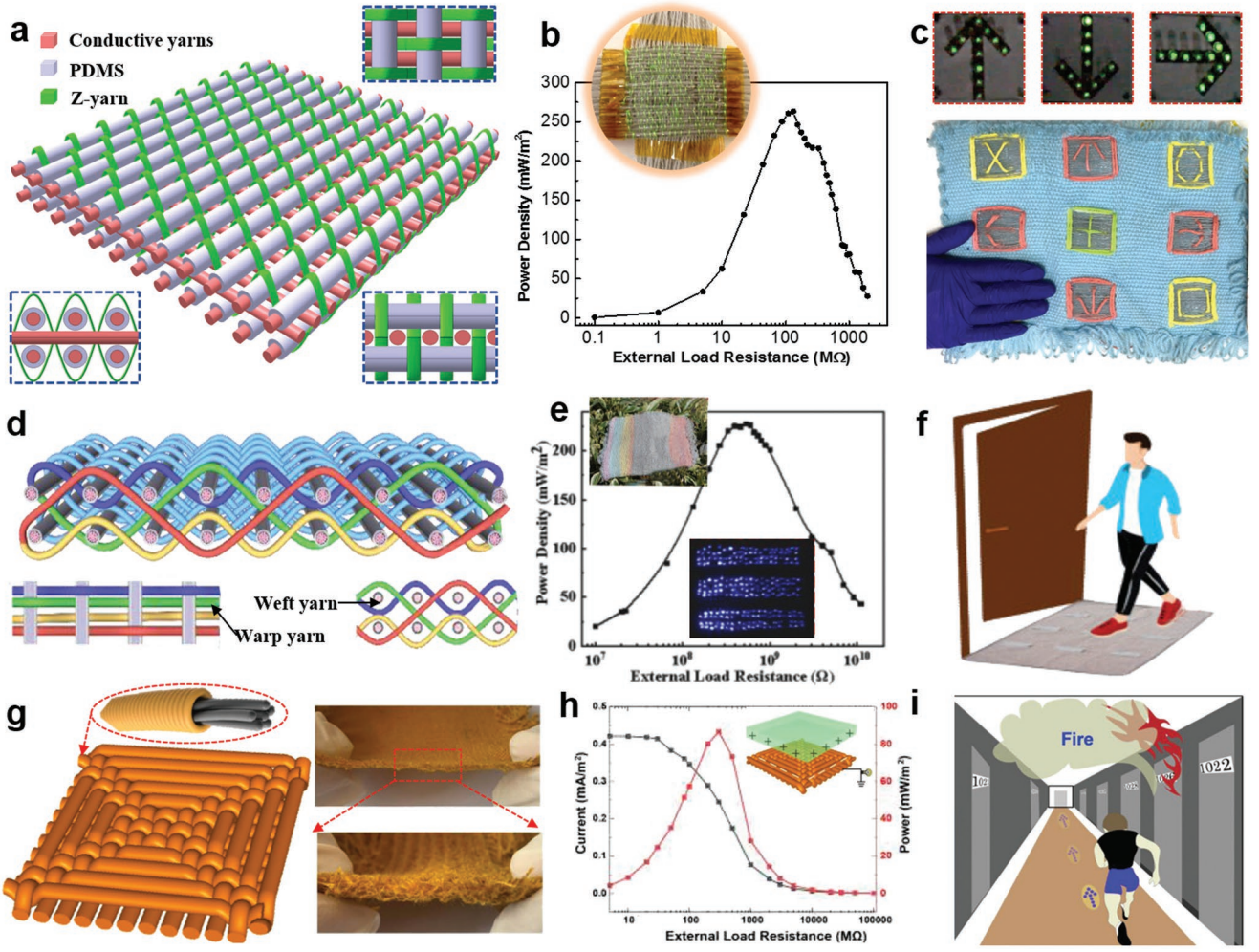

Figure 8. Structure designs and power output of 3D woven TENGs. a) Schematic illustration of a 3D orthogonal woven TENG (3DOW-TENG). b) Power density of the 3DOW-TENG under the tapping frequency of 3 Hz. A photograph of the test sample with the contact area of 45 × 40 mm^2 is shown in the top left. c) Demonstration of the 3DOW-TENG as a self-powered dancing carpet. a–c) Adapted with permission.[134] Copyright 2017, Wiley-VCH. d) Structural characteristic of a 3D angle-interlock woven TENG (3DAW-TENG). e) Power density of the 3DAW-TENG with the sample and the lighting LEDs shown in its top left and bottom, respectively. f) Schematic diagram of the smart carpet with the 3DAW-TENGs mounted on its surface. d–f) Reproduced with permission.[135] Copyright 2020, Elsevier. g) Schematic illustration and photograph of a 3D honeycomb woven TENG (3DHW-TENG). h) Current and peak power density of the 3DHW-TENG. i) Demonstration of the self-powered fire escape and rescue system. g–i) Reproduced with permission.[136] Copyright 2020, Wiley-VCH.

stretchable performance even the fabricated fibers without the intrinsic stretchable property, which can be stretched up to 30% (Figure 9bii). Under the vertical contact and separation mode, the maximum output power of 3DRK-TENG is 60 μW at the matched resistance of 5 MΩ (Figure 9b-iii). Furthermore, a 3D penetrated fabric TENG (3DP-TENG) is developed using a commercially 3D knitting fabric structure as a template, which has high elastic behavior in the thickness direction.[139] As shown in Figure 9c-i, the 3DP-TENG consists of a bottom surface coated with PDMS, and two thin layers of CNT sheet and silver paste that are then coated on the bottom and top surfaces as the two electrodes. The peak power of the 3DP-TENG with a size of 5 × 5 cm^2 can reach 153.8 mW m^{-2} at a load resistor of 1 GΩ (Figure 9c-ii). With the inherent features of large separation distance and high compression resilience, 3D spacer fabric is widely adopted to design textile TENGs.[140,141] For example, a 3D spacer fabric TENG (3DS-TENG) with weft knitting technology has been developed, which consists of two outer fabric layers and a spacer layer.[142] As illustrated in Figure 9d-i, polyester monofilament is used to knit the spacer layer due to its high stiffness, and nylon multifilament is used to knit two outer fabric layers. The 3DS-TENG exhibits excellent force sensitivity, which can be used to accurately recognize foot pressure (Figure 9d-ii,iii). Similarly, a scalable and washable 3D warp-knitted power fabric (3D-WSF) with high compressive resilience and good electrical output is developed.[143] The 3D-WSF with sandwich structure is composed of the top polyethylene (PE) braided layer, the middle poly(ethylene terephthalate) (PET) spacer layer, and the bottom poly(tetrafluoroethylene) (PTFE) braided layer, in which the spacer PET fibers interweave with PE and PTFE fibers up and down to form a coherent whole. Another kind of 3DS-TENG as a kind of all textile energy harvester is fabricated by a computerized

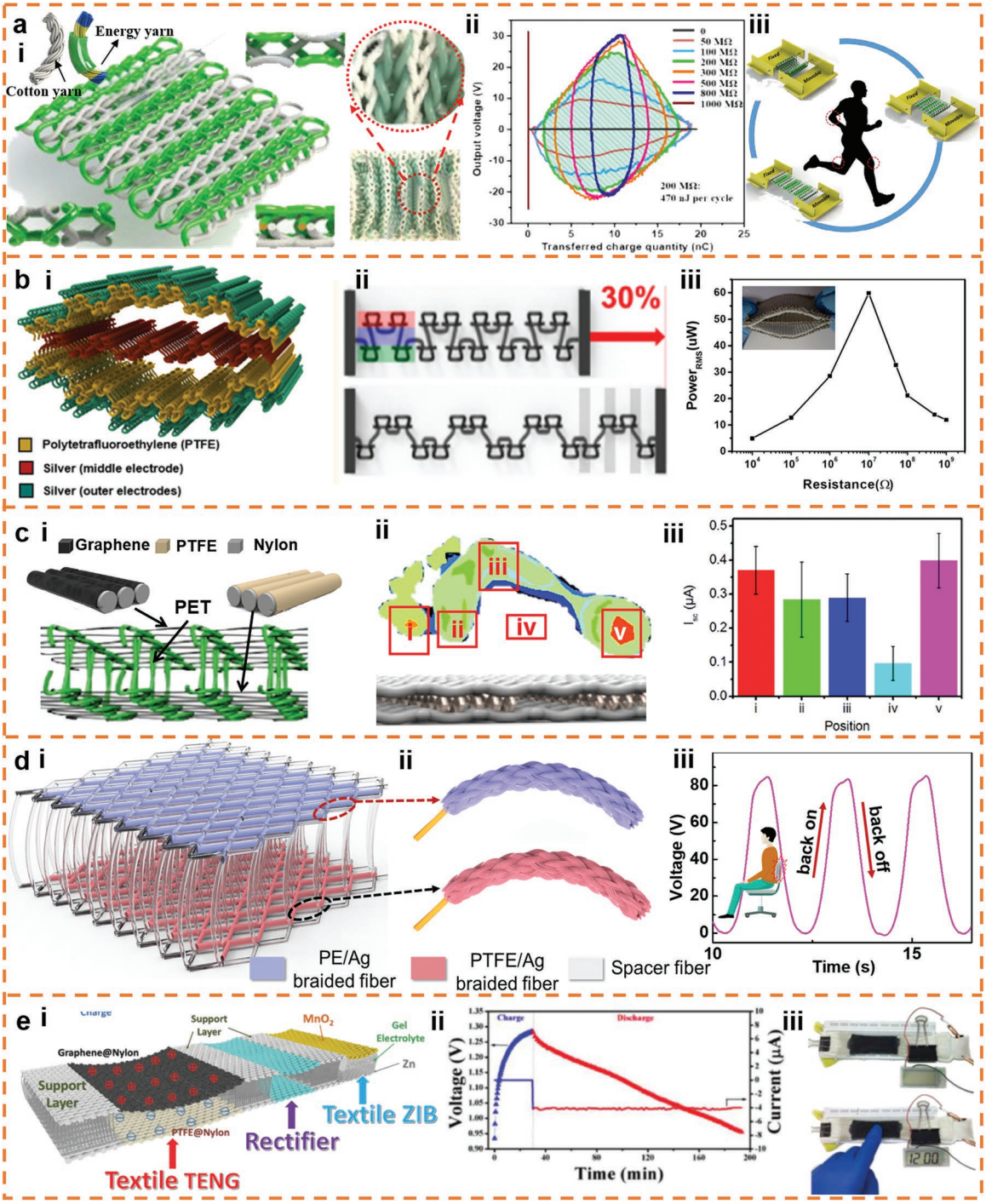

Figure 9. Architecture characteristics and output performance of 3D knitted TENGs. a) 3D double-faced interlock fabric TENG (3DFIF-TENG), including: i) illustration and photograph of the 3DFIF-TENG, ii) *V*–*Q* output of the 3DFIF-TENG with different external load resistances, and iii) schematic diagram of the 3DFIF-TENG under recycling tensile and release loading. Reproduced with permission.[137] Copyright 2020, Elsevier. b) Fully stretchable 3D rib-knitted fabric TENG (3DRK-TENG), including: i) 3D image of the 3DRK-TENG, ii) maximum elastic deformation of the 3DRK-TENG, and iii) average power output of the 3DRK-TENG in a vertical contact mode at the frequency of 3.3 Hz. Reproduced with permission.[138] Copyright 2017, American Chemical Society. c) 3D spacer fabric TENG (3DS-TENG), including: i) scheme of the 3DS-TENG, ii) pressure distribution of human foot, and iii) short-circuit current of the 3DS-TENG pixels located at different positions of the foot. Reproduced with permission.[142] Copyright 2016, Elsevier. d) Scalable and washable 3D warp-knitted spacer power fabric (3D-WSF) for energy harvesting and pressure sensing, including: i) 3D structural diagram of the 3D-WSF, ii) schematic illustration of the eight-axial PE and PTFE braided fibers both with conductive Ag-coated nylon fibers embedded in the center, iii) characteristic analysis of voltage signal in sitting posture monitoring. Reproduced with permission.[143] Copyright 2021, IOP Publishing. e) 3D self-charging spacer fabric (3DSC-TENG), including i) schematic diagram of the 3DSC-TENG, ii) charge/discharge characteristics of the 3DSC-TENG, and iii) demonstration showing an electronic watch powered by the 3DSC-TENG. Reproduced with permission.[145] Copyright 2018, Wiley-VCH.

flat knitting machine.[144] The top layer of 3DS-TENG is knitted with conductive silver-plated nylon fibers on one needle bed, and the bottom layer is knitted with PAN fiber on the other needle bed. The top layer and bottom layer are connected together with cotton fibers. The 3DS-TENG can greatly increase output power by increasing the contact separation distances. In order to realize continuous and stable electrical output, the integration of TENGs with flexible Zn-ion battery (ZIB) is embedded in a piece of 3D spacer fabric. As displayed in Figure 9e-i, the 3D spacer fabric consists of three layers, of which the upper and lower layers are spaced apart.[145] Fabric TENGs work with the motion of up and down layers, and the batteries with the three layers are fabricated by injecting the electrolyte into the intermediate layer, which can convert human mechanical energy into electrical energy, and further store the electric energy in the battery to supply power for various electronic devices (Figure 9e-ii,iii). Through the above introduction, it can be found that 3D knitted structures are very popular to design textile TENGs due to their high permeability and elasticity.

7.3. 3D Braided Structures

3D braided fabric consists of multiplied braided yarn by moving and interweaving with each other in different directions, which can be classified into four or five directional structures based on the number of braided yarns. The intertwined structure of 3D braided fabric endows it with the merits of high flexibility, structural integrity, shape adaptability, and mechanical stability. Recently, a 3DB-TENG with good air permeability, high compression resilience, enhanced power output, improved pressure sensitivity, and machine washability is developed, which can combine the merits of both 3D braided fabric and TENGs.[60] As shown in **Figure 10**a, the 3DB-TENG is fabricated through a four-step rectangular braiding technology, using the PDMS-coated energy yarn as the braided yarn and the eight-axial winding yarn as the axial yarn. Particularly, numerous rhombus-shaped frame-column structures are established between the outer braided braced frame and the inner core column, which provide high

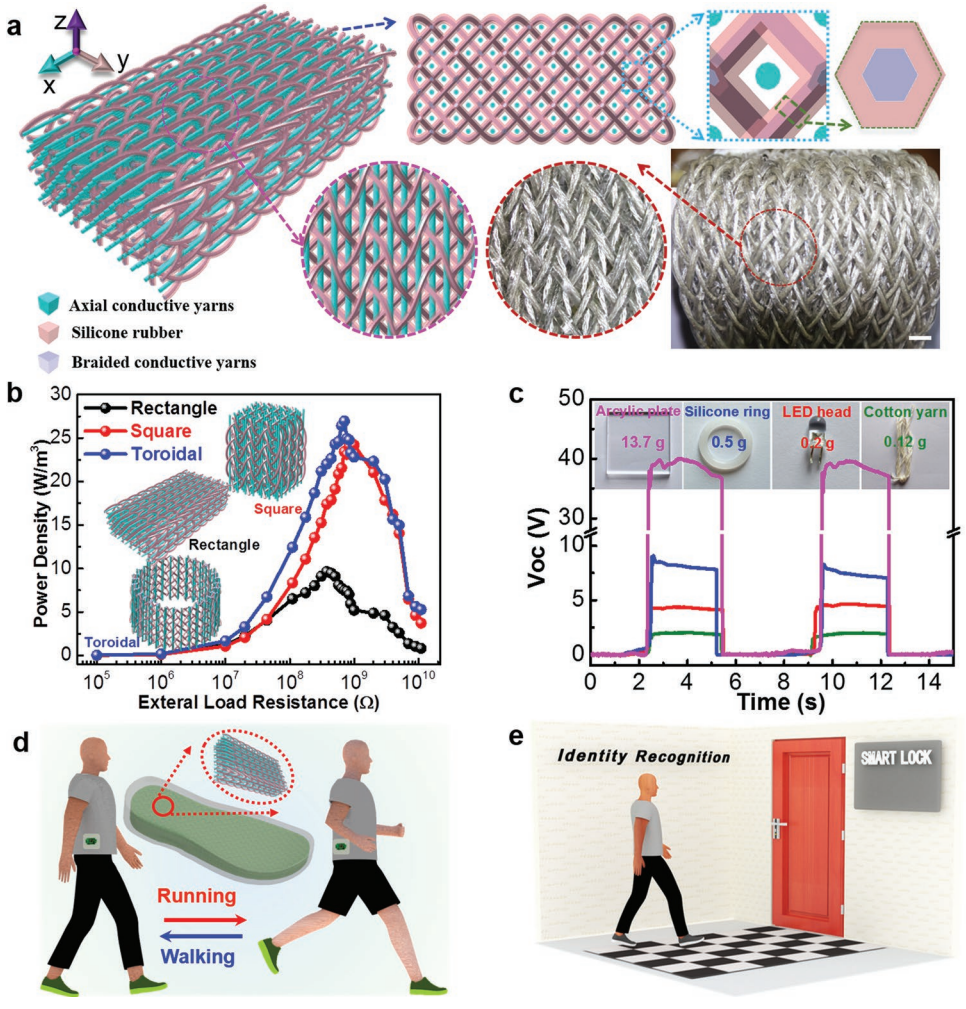

Figure 10. Shape adaptable and highly resilient 3D braided TENG. a) Structural characteristic of 3D braided TENG, including the outer braided braced frame and the inner axial core column. b) Comparison of the power densities of the 3D braided TENGs with different cross-sectional shapes. c) Pressure sensitivity of the 3D braided TENG to different objects. d,e) Applications of the 3D braided TENG as an intelligent footwear system (d) and a self-powered identity recognition system (e). a–e) Reproduced under the terms of the CC-BY Creative Commons Attribution 4.0 International license (https://creativecommons.org/licenses/by/4.0).[60] Copyright 2018, The Authors, published by Springer Nature.

compression resilience and improved working performance of the 3DB-TENG. In addition, by adjusting the arrangement of yarns on the machine bed, the cross section of 3DB-TENG can be adjusted, such as rectangle shape, square shape, and toroidal shape. Among the three cross-sectional structures, the toroidal shape has the highest power output density, which can reach 26 W m^{-3} under the loading frequency of 3 Hz and the applied force of 20 N (Figure 10b). Moreover, the 3DB-TENG can repeatedly and steadily distinguish the difference of electrical signal even if the mass variation is less than 0.1 g (Figure 10c). Finally, the 3DB-TENG is applied to two new forms of human–machine interactive applications, including an intelligent shoe for human motion monitoring and a self-powered identity recognition carpet for safeguarding entrance, as shown in Figure 10d,e, respectively. This work provides a new design concept of 3D five-directional braiding structure and several innovative application occasions for 3D braided TENGs. However, compared with other 3D fabrics, more complicated preparation process and longer production cycles lead to higher cost of 3D braided fabrics. In addition, although the axial length of 3D braided fabric can be extended infinitely in theory, it is difficult to expand its plane size in a large area due to the limitation of the number of yarn spindles.

7.4. 3D Nonwoven Structures

3D nonwoven fabrics with numerous hierarchical porous structures are usually obtained by stacking multiple layered 2D nonwoven nanofiber films, membranes, webs, nets or felts in thickness direction. Because of excellent flexibility, air permeability, and conformability, 3D nonwovens have attracted extensive attentions, which have great potentials in energy harvesting and pressure sensing. For example, by sandwiching silver nanowires (Ag NWs) between poly(lactic-*co*-glycolic acid) (PLGA) nanofiber film and poly(vinyl alcohol) (PVA) nanofiber film, the breathable, biodegradable, antibacterial and self-powered electronic skin based on all nanofiber TENG is fabricated (**Figure 11**a).[146] The maximum areal power density of the PLGA/Ag NWs/PVA e-skin is ≈130 mW m^{-2} at a matched resistance of ≈500 MΩ, which is four times more than that of the PVA/Ag NWs/PVA e-skin (Figure 11b). The designed e-skin can realize real-time and self-powered monitoring of physiological signals and joint movement of the whole body (Figure 11c). In addition, based on the similar configuration of all nanofibers, a self-powered e-skin for real-time respiration monitoring is designed.[112] Figure 11d exhibits the application scenario and 3D structure diagram of the self-powered all-nanofiber e-skin, which consists of polyamide 66 (PA 66) nanofibers coated with Au electrode as the top electrification layer and Au electrode coated polyacrylonitrile (PAN) nanofibers as the bottom electrification layer. The all-nanofiber respiratory monitoring e-skin is also used for the diagnosis of obstructive sleep apnea–hypopnea syndrome (Figure 11e). Figure 11f shows the electrical signal characteristics of three typical respiratory states, including normal breathing, sleep hypopnea, and sleep apnea, from which it can be observed that the voltage amplitude decreases significantly, indicating the occurrence of obstructive respiratory events. The apnea–hypopnea index defined as the total number of apneas and hypopneas per hour of sleep is also an index to evaluate the degree of obstructive sleep apnea–hypopnea syndrome, which helps to improve sleep quality and human respiratory health. There are many similar studies on TENGs based on multifunctional all nanofibers, which have air permeability, ultraviolet protection, self-cleaning, antibacterial and self-powered properties, that are fabricated based on a low-cost and facile electrospinning method.[147,148] In addition to the above functionalities, ferroelectric materials, such as PVDF and its derivatives can also be incorporated into nanofibers by means of electrospinning techniques to improve the power output of TENGs. For instance, an all-fiber tribo-ferroelectric synergistic e-skin with high power output and thermal-moisture comfortability is developed, as shown in Figure 11g.[149] The e-skin consists of four function layers, including PVDF-TrFE nonwoven webs and polyamide 6 (PA6) nonwoven webs with opposite tribo-polarity for contact electrification, nickel–copper (Ni–Cu) fabric electrode for charge induction, and the moisture-wicking fabric for directional water transport and evaporation, as demonstrated in Figure 11h. Owing to the tribo-ferroelectric synergistic effect induced by PVDF-TrFE, the maximum peak power density of the e-skin can reach 5.2 W m^{-2} under the loading frequency of 2.5 Hz. Another similar work has also been reported.[150] As presented in Figure 11i, the multilayer nanofiber stacked smart fabric is composed of a ferroelectric-enhanced TENG and a directional moisture-wicking fabric. When running from human skin to the environment, large-sized water clusters will be decomposed into small-sized water clusters or water monomers to increase the rate of water evaporation. Figure 11j shows the electrical output performance of the fabric, whose maximum instantaneous power density is about 135 W m^{-3} at the matched resistance of 60 MΩ. The quick-drying and cooling fabric can be further used as a wireless sports monitoring insole to reduce the skin temperature when walking (Figure 11k). In addition to the above, there are many other reported TENGs with 3D nonwovens, which contain various functional attributes.[151–154] Considering that many polymers can be easily prepared into nanofibers by electrospinning, it is very popular that 3D nonwovens can integrate multiple functions, which is more suitable for the design of skin-like sensors.

7.5. 3D Printing Structures

In addition to the pervasive 3D structures manufactured with traditional textile techniques, 3D printing technology with the benefits of being simple, adaptable, cheap, fast, efficient, durable, sustainable, and precise has also been widely leveraged for the fabrication of wearable electronics with irregular and complex shapes in a one-step integration way.[155–157] The integration of advanced TENG with burgeoning 3D printing technology and traditional textile structures fosters the emergence of 3D printing textile-based TENGs. For example, 3D printed elastomeric metal-core silicone–Cu TENG fibers are fabricated by using a coaxial microextrusion process (**Figure 12**a). Continuous extrusion of silicone in combination with continuous vertical motion of the extruder results in the production of metal-core elastomeric silicone–Cu fiber TENGs (Figure 12b). With the help of different shapes of substrates, various kinds

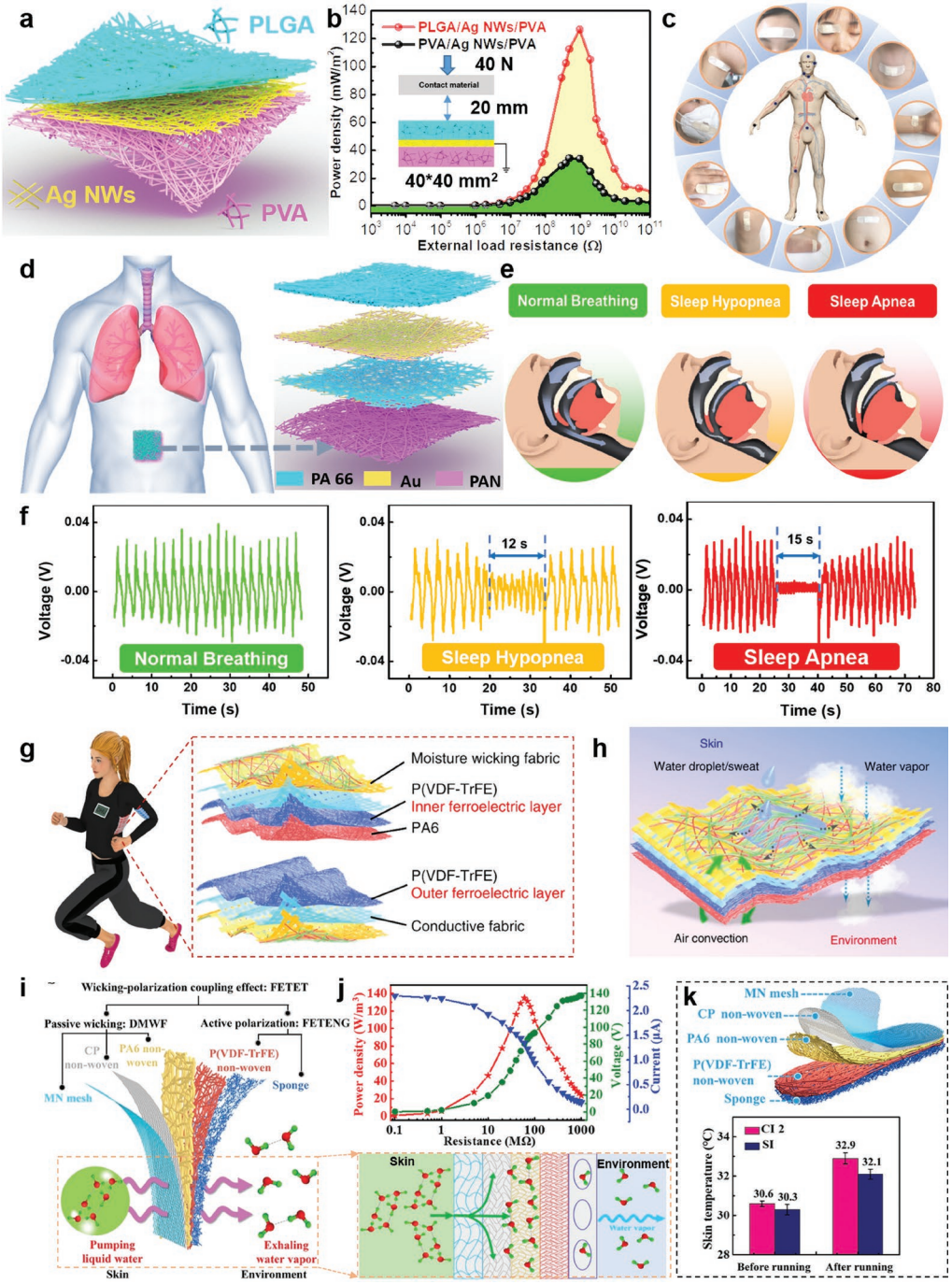

Figure 11. 3D multilayered nonwoven TENGs as multifunctional electronic skins. a) Schematic illustration of the 3D network structure of an all-nanofiber TENG-based e-skin. b) Peak power density of the TENG-based e-skin under varied external resistance c). a–c) Adapted with permission.[66] Copyright 2020, AAAS. Reprinted/adapted from ref. [66]. © The Authors, some rights reserved; exclusive licensee American Association for the Advancement of Science. Distributed under a Creative Commons Attribution NonCommercial License 4.0 (CC BY-NC) https://creativecommons.org/licenses/by-nc/4.0/. The photos appear here with the subject's consent. d) Application scenario and schematic illustration of a self-powered all-nanofiber e-skin. e) Respiratory airway states while asleep. The left, middle, and right images are normal, narrowed, and closed airways, respectively. f) Real-time voltage signals under different sleep respiratory states, including normal, hypopnea, and apnea. d–f) Reproduced with permission.[112] Copyright 2021, Wiley-VCH. g) Structural diagram of an all-fiber tribo-ferroelectric synergistic e-skin. h) Schematic illustration showing that the all-fiber TENG-based e-skin with the functions of breathability, moisture permeability, and moisture wicking. g,h) Reproduced under the terms of the CC-BY Creative Commons Attribution 4.0 International license (https://creativecommons.org/licenses/by/4.0).[149] Copyright 2018, The Authors, Published by Springer Nature. i) Schematic structure of the ferroelectric-enhanced triboelectric evaporation textile and the water transport path on the skin under the wicking-polarization coupling effect. j) Electrical output performance of the textile TENG measured at different external load resistances. k) Schematic diagram of a smart insole and its application in skin surface cooling function. i–k) Reproduced with permission.[150] Copyright 2021, Wiley-VCH.

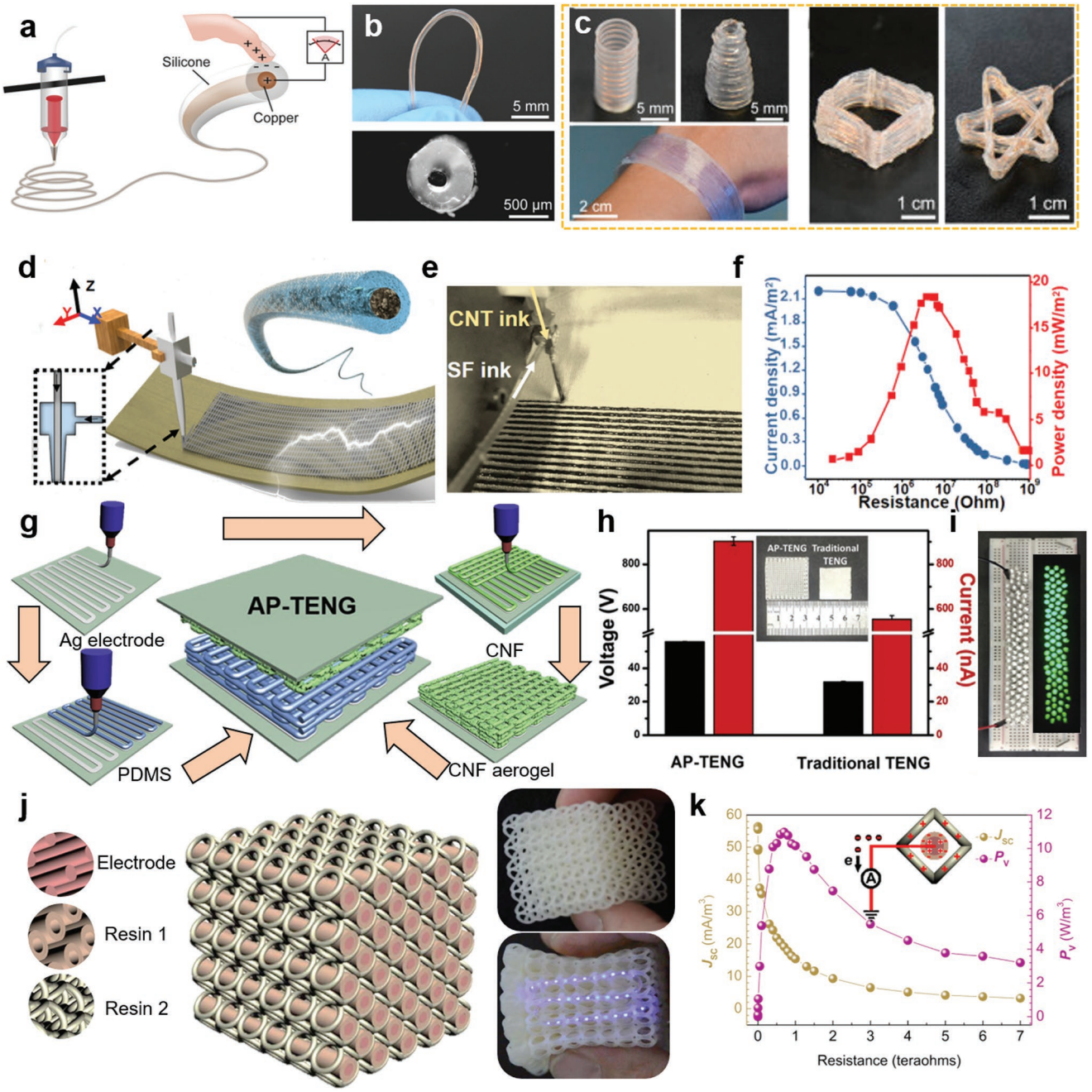

Figure 12. 3D printing fabric TENGs. a) Schematic illustration of 3D printing triboelectric fibers. b) Surface and cross-sectional photographs of 3D printing triboelectric fibers. c) Photographs of 3D printing structures with different shapes. a–c) Reproduced with permission.[158] Copyright 2020, Elsevier. d) Schematic illustration showing the 3D printing process using a coaxial spinneret. e) Photograph of the 3D printing process. f) Short-circuit density and power density as a function of resistances of the 3D printed smart textile. d–f) Reproduced with permission.[159] Copyright 2019, Elsevier. g) Schematic fabrication process of all printed TENG (AP-TENG). h) Output comparison between 3D hierarchical patterned AP-TENG and mold-cast flat microporous TENG counterpart. i) Demonstration of lighting up 88 commercial LEDs connected in series. g–i) Reproduced with permission.[160] Copyright 2019, Elsevier. j) Overall structure of a 3D ultraflexible TENG. k) Current density and peak power density of the 3D ultraflexible TENG under the frequency of 1.3 Hz. j,k) Reproduced with permission.[161] Copyright 2018, Elsevier.

of 3D-printed flexible structures with hollow cylinder, cone, cuboid and star shapes have been fabricated,[158] as demonstrated in Figure 12c. Besides the fiber-shaped TENGs, 3D printing can also be used to directly 3D fabric TENGs or other complex structural TENGs. For instance, by employing a 3D printer equipped with a coaxial spinneret, core-sheath fibers are directly printed on the e-textiles (Figure 12d). The printed fibers choose CNTs as the conductive core layer and silk fibroin (SF) as the dielectric sheath to fabricate CNTs@SF core-sheath fiber-based smart pattern (Figure 12e).[159] The CNTs@SF

fiber-based smart textile can achieve a maximal power density of 18 mW m^{-2} at an external resistance load of 4 MΩ under a displacement speed of 10 cm s^{-1} (Figure 12f). Similarly, an all-printed TENG (AP-TENG) with micro-3D pattern and nanoporous aerogel structure is designed and fabricated through a fully direct-write printing approach.[160] As illustrated in Figure 12g, CNF ink and PDMS ink are printed onto Ag/PET substrates, respectively, forming 3D patterned positive and negative friction layers. As shown in Figure 12h, the output voltage and current of the 3D AP-TENG are both higher than those of traditional 2D flat TENG, indicating a superior electrical output performance of the 3D AP-TENG. The power generation demonstration of the 3D AP-TENG shows that it can light up 88 commercial LEDs connected in series (Figure 12i). One of the most outstanding advantages of 3D printing is the rapid design ability of complex structures. As exhibited in Figure 12j, a practical and ultraflexible 3D printing TENG is reported which consists of printed composite resin parts and ionic hydrogel as the electrification layer and electrode, respectively.[161] It is found that an instantaneous peak power density of 10.98 W m^{-3} and a transferred charge density of 0.65 mC m^{-3} are achieved under a low frequency of about 1.3 Hz (Figure 12k). A self-powered SOS flicking and buzzing distress signal system is demonstrated to show its potential applications in wearable electronic devices.

7.6. 3D Multilayer Fabric Stacking Structures

Similar to most reported TENGs fabricated with multilayer composite film structure to improve their performance,[103,162,163] one of the simplest strategies to prepare high-performance 3D fabric TENGs is to combine or stack multiple single-layer functional fabrics in a certain order. Therefore, 3D fabric TENGs with multilayer fabric stacking structures have also been widely reported. For example, a narrow-gap textile TENG stitched face to face with nonconductive textiles is composed of two composite layers, one of which is a thin and wrinkled nitrile film attached to a conductive textile, the other of which is a conductive textile coated with silicone rubber,[164] as shown in **Figure 13**a. The electricity generated from the textile TENG is further used to stimulate the sciatic nerve of rats for potential application in implantable and self-powered rehabilitation system (Figure 13b). Additional functions can also be well and easily integrated into the 3D multilayer fabric stacking systems. One example is the self-extinguishing flame-retardant fabric TENG for fire protection applications, which consists of two flame-retardant silver-coated cotton fabrics, a PTFE-coated cotton fabric, and an intermediate divider (Figure 13c).[165] Under an external load resistance of 700 MΩ, the maximum peak output power density of the flame-retardant TENG can achieve 343 mW m^{-2} (Figure 13d). Owing to the excellent fire resistance and power output ability, the flame-retardant fabric TENG is applied for firefighter self-rescuing system and forest fire warning system (Figure 13e). In addition, fabric TENGs with multilayer fabric stacking structure are also used in the fields of human–machine interfaces. For example, a fully fabric TENG used as self-powered human–machine interactive keyboard is composed of the top PTFE-coated PET cloth, the middle CNT coated cotton fabric, and the bottom silver pasted PET cloth (Figure 13f).[166] The peak power density of the fabric TENG is 3.8 mW m^{-2} at the resistance of 1 GΩ and contact frequency of 1 Hz (Figure 13g), which is able to light up dozens of LEDs and charge capacitors. The self-powered wearable keyboard is further demonstrated in the biometric recognition system to identify visitors (Figure 13h). Recently, a hydrophobic self-repairing power textile with multilayer fabric stacking structure has been designed for water droplet energy harvesting (Figure 13i).[167] The obtained voltage output of the power textile is improved about seven times than that of traditional single-electrode mode TENG (Figure 13j). As a result, the power textile under one water droplet can power 25 LEDs, demonstrating its ability to power wearable electronics (Figure 13k). From these examples, it can be seen that 3D multilayer fabric stacking structure is a relatively simple and rapid method to prepare functional textile TENGs. In addition, with the help of large-area surface-to-surface contact, the power output of 3D multilayer stacking structural fabrics is high. However, the instability between interlayer interfaces leads to poor mechanical and working stability of textile TENGs.

8. Comparison the 3D Fabric TENGs with 2D Fabric and 1D Fiber TENGs

It is well known that autonomous power supply and self-powered sensing are the two most prominent functions of TENGs. Accordingly, power density and pressure sensitivity are the two key indexes to investigate the overall properties of TENGs. With the purpose of fully grasping the development trend of TENGs in the two indicators in recent years, the peak power density and pressure sensitivity of TENGs with curved fiber structures are first summarized with the focus on comparing with planar membrane structures.[24,83,113,135,144,168–183] As shown in **Figure 14**a,b, the overall variation of the two metrics shows an upward trend due to the improved structural design and fabrication process. In addition, TENGs with planar membrane structures present higher power density and pressure sensitivity than those with curved fiber structures. Moreover, with the advancement of relevant research, this trend will become more obvious. The potential reason can be attributed to the difference of effective contact area. Planar membrane structures can achieve more full and faster contact with external objects than curved fiber structures, resulting in more and easier charge transfer. Therefore, it can be concluded that effective contact area plays a crucial role in electrical output and pressure sensing of TENGs. In order to compare the output performance differences of textile TENGs caused by the difference of textile structure dimensions, the two main technique indicators, such as peak power density and pressure response sensitivity, of various textile-structured (1D fibers, 2D fabrics, and 3D fabrics) TENGs are systematically compared, as presented in **Table 4**. Based on these literature data, a regional distribution map with the peak power density and pressure sensitivity as the abscissa and ordinate, respectively, is further plotted in Figure 14c, in which the regions of 1D fiber TENGs, 2D fabric TENGs, and 3D fabric TENGs are marked with green, red and blue color, respectively. It can be found that 3D power fabrics exhibit generally higher electrical output and pressure response

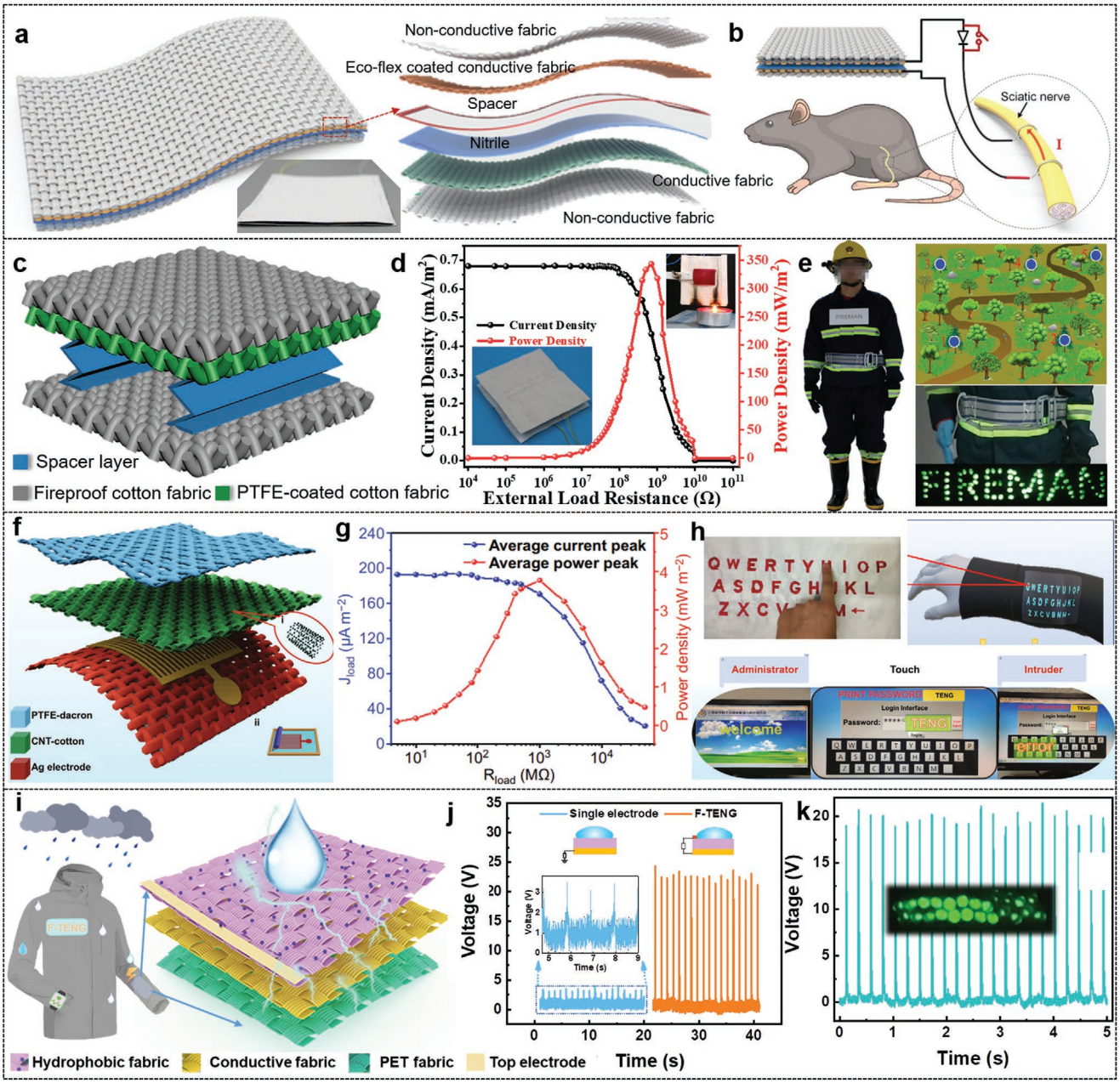

Figure 13. 3D multilayer fabric stacking TENGs. a) Illustration of wearable textile TENG for the next-generation healthcare applications. b) Rehabilitation application for direct nerve stimulation. a,b) Reproduced under the terms of the CC-BY Creative Commons Attribution 4.0 International license (https://creativecommons.org/licenses/by/4.0.[164] Copyright 2019, The Authors, published be Wiley-VCH. c) Schematic diagram of the flame-retardant textile-based TENG. d) Output current density and power density of the flame-retardant TENG with external resistances. e) Applications of the flame-retardant TENG for forest self-rescue and fire location alarm system. c–e) Reproduced with permission.[165] Copyright 2020, American Chemical Society. f) Structural design of the fabric-based TENG. g) Current density and power density of the fabric TENG varying with external resistances. h) Application of the fabric TENG for user login identification. f–h) Reproduced under the terms of the CC-BY Creative Commons Attribution 4.0 International license (https://creativecommons.org/licenses/by/4.0).[166] Copyright 2021, The Authors, Published by Springer Nature. i) An all-fabric TENG with hydrophobic self-repairing ability for water droplet energy harvesting. j) Comparison of voltage output between traditional single-electrode mode TENG and the developed all fabric TENG. k) Demonstration of powering LED arrays under one water droplet. i–k) Reproduced with permission.[167] Copyright 2021, American Chemical Society.

performance than 1D energy fibers and 2D power fabrics, which gives clear evidence that 3D fabric TENGs have more potential to achieve higher power density and better pressure sensitivity than 1D fiber TENGs and 2D fabric TENGs. The electrical or signal generation of TENGs mainly comes from contact electrification or triboelectrification between two materials. For fiber/fabric-structured TENGs, charge transfer may occur in four contact pairs, including between conductive and dielectric

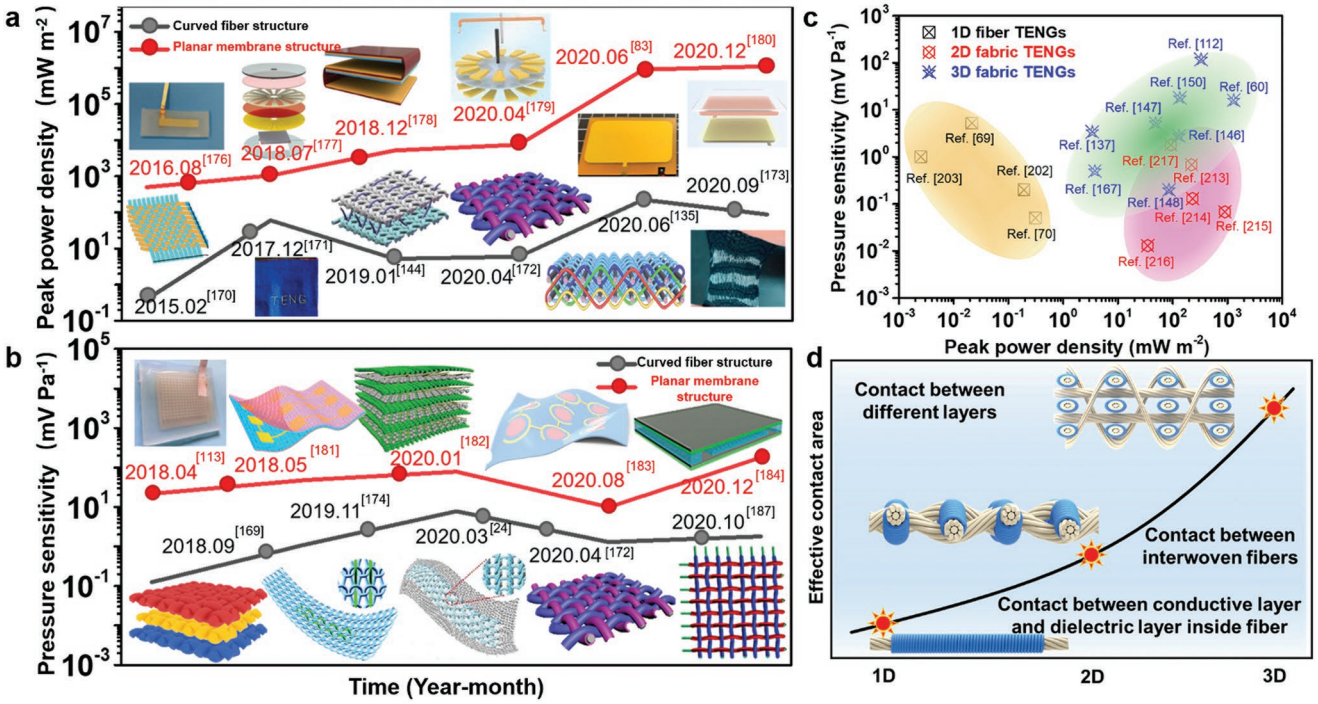

Figure 14. Investigation of the advantages of 3D fabrics in power output and pressure response compared with 1D fibers and 2D fabrics. a) Comparison of peak power density between curved fiber structure and planar membrane structure in recent years. b) Comparison of pressure sensitivity between curved fiber structure and planar membrane structure in recent years. c) Comparison of power output and pressure sensing abilities among 1D fibers, 2D fabrics, and 3D fabrics. d) Qualitatively comparison of effective contact area among 1D fibers, 2D fabrics, and 3D fabrics.

materials inside fibers, between in-plane fibers with orthogonal or arbitrarily orientation, between fibers in different layers, and between surface fibers and external objects. In addition to contact with external objects, the other three contact pairs only exist in the fiber/fabric system. As shown in Figure 14d, the effective contact area shows an exponential growth trend with the extension of textile structure system from 1D fibers to 2D fabrics and then to 3D fabrics. In 1D fiber TENGs, the charge transfer comes from the interface between the core electrode and the sheath dielectric layer. When multiple 1D energy fibers are combined into fabrics through various processes, the interweaving of fibers with different orientations will greatly increase the contact area. Furthermore, by increasing the number of fabric stacking layers in the thickness direction, 3D fabric TENGs add additional interlayer contact area on the basis of 1D fibers and 2D fabrics. Therefore, 3D fabric TENGs with a larger effective contact area than 1D fiber TENGs and 2D fabric TENGs show higher power output and electrical response performance, which have better application prospects in autonomous power sources and self-powered sensors.

9. Summary and Outlook

High power output and high sensing sensitivity are the eternal pursuit of TENGs, which can be improved through a variety of strategies involving constitutive theory, material modification, interface optimization, structural design, circuit management, system integration, and so on. Although the electromechanical conversion performance of TENGs has steadily improved, the power output and sensing ability of textile TENGs are far behind those of common membrane TENGs, owing to their special curved surfaces and micro-to-nano defect structures. In order to provide comprehensive summary and methodological guidance for the future high-performance energy and sensing textiles, TENGs with advanced 3D fabric structures are discussed in detail, with emphasis on the fabrication processes and structural characteristics, including weaving, knitting, braiding, nonwoven, printing, and multilayer stacking. Particularly, the operating modes and working mechanisms of TENGs are reinterpreted from the perspective of the structural characteristics of fibers or fabrics. In addition, some commonly used approaches to improve the electromechanical conversion performance of TENGs are also summarized. Finally, peak power density and pressure response sensitivity as the two key indicators of TENGs are compared between the curved fiber structure and planar membrane structure, as well as among 1D fibers, 2D fabrics, and 3D fabrics. The potential reason for the inferior electromechanical conversion ability of textile TENGs is revealed, which is due to the difference in contact electrification caused by effective contact area.

Based on the above comprehensive understanding of the state of the art of 3D fabric TENGs, it is obvious that 3D fabrics are far better than 1D fibers and 2D fabrics in terms of electromechanical conversion performance, which have more potential to realize high-performance energy and sensing textiles. Another remarkable advantage of 3D fabric is that it is also a powerful combination platform for multifunctional integration. As the application scenario illustrated in **Figure 15**, it can realize efficient acquisition and synchronous storage of multiple energy forms, as well as real-time response and self-powered sensing of

Table 4. Comparison of electrical output and pressure sensitivity among 1D, 2D and 3D textile-based TENGs.

Structural dimension	Fabrication method	Working mode	Electrode material	Electrification material	Peak power density (loading conditions)	Pressure sensitivity	Ref.
1D	Dip-coating	SE	Ag NPs/MXene	PDMS	–	1 mV Pa^{-1}	[200]
1D	Dip-coating/conformal coating	SE	CNTs/Ag NWs mixed	PDMS	21.5 μW m^{-1} (1.5 GΩ, 1 Hz, 20 N)	5.2 mV Pa^{-1}	[69]
1D	Injecting	SE	Liquid metal	Silicone rubber/PCMs	192 μW m^{-1} (150 MΩ, 1 Hz, 20 N)	0.2 mV Pa^{-1}	[201]
1D	Core-sheath inserting	CS	Silver-coated nylon fiber	Silicone rubber	311 μW m^{-1} (300 MΩ, 3 Hz, 20 N)	0.05 mV Pa^{-1}	[68]
1D	Core-sheath inserting	SE	Silver fiber	PDMS	2.5 μW m^{-1} (40 MΩ, 3 Hz)	1 mV Pa^{-1}	[202]
1D	Conjugate spinning	SE	Conductive fiber	Latex/PVDF-TrFE	432 μW m^{-1}	–	[203]
1D	Thermal drawing	SE	Tungsten wire	PP tubing with acrylic	43 mW kg^{-1} (80 MΩ, 8 Hz, 70 N)	–	[204]
1D	Electrospinning	SE	Silver-coated nylon fiber	PAN@PVDF	336 μW m^{-1} (500 MΩ, 2.5 Hz)	–	[205]
1D	Injecting	SE	Liquid metal (EGaIn)	SEBS hollow fiber	360 μW m^{-1} (100 MΩ, 4 Hz, 0.1 N)	–	[206]
2D	Weft-knitting	CS	Silver-coated nylon fiber	PA66/PTFE	7.5 mW m^{-2} (40 MΩ, 2 Hz)	–	[207]
2D	Vacuum pumping/ plain woven	CS	Liquid metal (Galinstan)	Silicone rubber	30.4 mW m^{-2} (7 MΩ, 1 Hz)	–	[208]
2D	Weft-knitting	SE	Organogel electrode	Silicone hollow fiber	40 mW m^{-2} (300 MΩ, 3 Hz, 25 N)	–	[209]
2D	Plain woven	SE	Stainless steel fiber	Polyurethane fiber	60 mW m^{-2} (200 MΩ)	–	[170]
2D	Weft-knitting	SE	Stainless steel/polyester fiber	Silicone rubber	85 mW m^{-2} (100 MΩ, 3 Hz, 20 N)	–	[58]
2D	Wet-spinning	SE	PNA hydrogel fiber	Poly(methyl acrylate)	88 mW m^{-2} (200 MΩ, 1.25 Hz)	–	[172]
2D	Doctor bladed	CS	Ag NWs	TPU/PLA	1.25 W m^{-2} (200 MΩ, 1.25 Hz)	–	[210]
2D	Electrospinning/plain woven	FT	Stainless steel fiber	PA66/PVDF-TrFE	93 mW m^{-2} (10 MΩ, 3 Hz, 200N)	1.8 mV Pa^{-1}	[211]
2D	Electrospinning	SE	Liquid metal-Ag flakes	PVDF-HFP/SEBS	220 mW m^{-2} (20 MΩ, 5 Hz, 30N)	0.68 mV Pa^{-1}	[212]
2D	Plain knitting	SE	Stainless steel fiber	Nylon fiber	–	7.8 mV Pa^{-1}	[24]
2D	Yarn winding and embedding	SE	Silver-coated nylon fiber	Silicone rubber	230 mW m^{-2} (100 MΩ, 3 Hz, 20N)	0.13 mV Pa^{-1}	[62]
2D	Electrospinning nano-fiber mat	CS	Copper	PDMS ion gel/PVDF-TrFE	900 mW m^{-2} (10 KΩ)	0.068 mV Pa^{-1}	[213]
2D	Plain woven	SE	Silver-coated nylon fiber	Tencel/chitosan blended fiber	15.8 mW m^{-2} (70 MΩ, 3 Hz, 100N)	1.94 mV Pa^{-1}	[214]
3D	Double-faced interlock	CS	Silver-coated nylon fiber	Cotton/silicone rubber	3.4 mW m^{-2} (200 MΩ)	3.4 mV Pa^{-1}	[137]
3D	Electrospinning non-woven web	SE	Carbon nanofibers	PVDF	85.4 mW m^{-2} (50 MΩ)	0.2 mV Pa^{-1}	[148]
3D	Electrospinning non-woven web	SE	Ag NWs	PLGA	130 mW m^{-2} (500 MΩ, 3 Hz, 20 N)	2.8 mV Pa^{-1}	[146]
3D	Electrospinning non-woven web	SE	Ag NWs	PAN/PTFE	48.6 mW m^{-2} (4160 MΩ, 1 Hz, 2 N)	5.2 mV Pa^{-1}	[147]
3D	Penetrated structure	CS	CNTs/Ag	PET/PDMS	153.8 mW m^{-2} (1 GΩ)	–	[139]
3D	Orthogonal woven	CS	Stainless steel/polyester fiber	PDMS	260 mW m^{-2} (132 MΩ, 3 Hz, 20 N)	–	[134]
3D	Angle-interlock woven	CS	GO	Silicone rubber	225 mW m^{-2} (700 MΩ, 1Hz)	–	[135]
3D	Computerized flat knitting	SE	Silver-plated nylon fiber	PAN	1768.2 mW m^{-2} (50 MΩ, 1200N)	–	[144]
3D	Electrospinning non-woven web	CS	Silver-coated nylon fabric	PA6/PVDF-TrFE	5.2 W m^{-2} (2.5 Hz)	–	[149]
3D	Electrospinning	CS	PA66/PAN	Au	330 mW m^{-2} (100 MΩ, 3 Hz)	0.217 kPa^{-1}	[112]
3D	Additive manufacturing	SE	PAAm-LiCl hydrogel	Composite resin	10.98 W m^{-3} (750 MΩ, 1.3 Hz)	–	[161]
3D	Fabric stacking	CS	Ag	PTFE/Ag	343 mW m^{-2} (700 MΩ, 3 Hz, 30 N)	–	[165]
3D	Spacer warp-knitted	CS	Silver-coated nylon fiber	Polyethylene/ poly(tetrafluoroethylene)	2.6 mW m^{-2} (100 MΩ, 3 Hz, 20 N)	–	[143]
3D	Fabric stacking	CS	CNT/Ag	PTFE	3.8 mW m^{-2} (1 GΩ, 1 Hz)	0.5 mV Pa^{-1}	[166]
3D	Four-step braiding	CS	Silver-coated nylon fiber	PDMS	26 W m^{-3} (3 Hz, 20 N)	16 mV Pa^{-1}	[60]
3D	Electrospinning nonwoven web	SE	Conductive sponge	PVDF-TrFE/silicone rubber	135 W m^{-3} (60 MΩ, 1.8 Hz)	18 mV Pa^{-1}	[150]

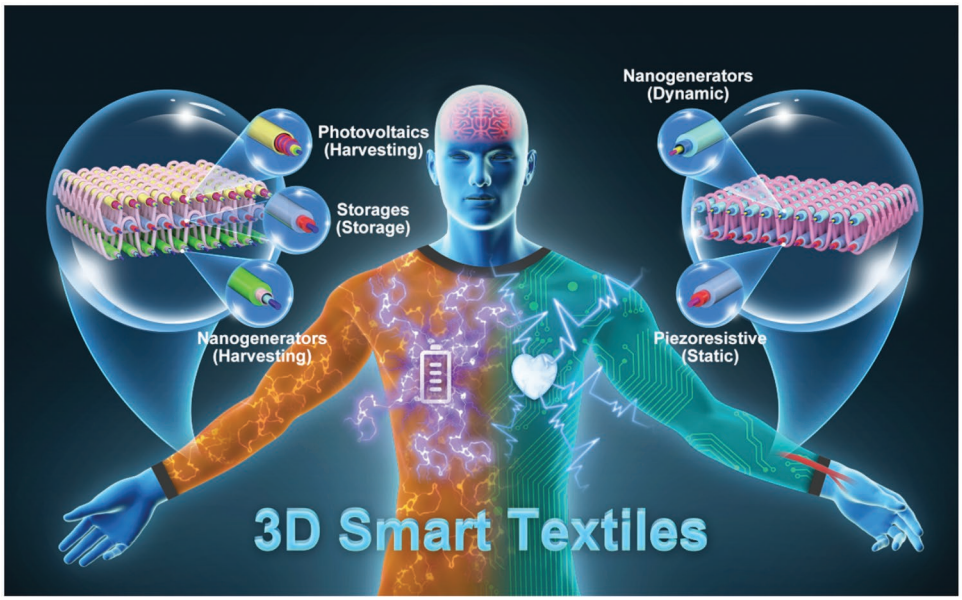

Figure 15. Two forward-looking/prospective research directions of smart textiles with novel 3D fabric structures. The 3D fabric structure on the left demonstrates efficient acquisition and synchronous storage of multiple energy forms that consist of the top photovoltaic collection layer, the middle electrochemical energy storage layer, and the bottom biomechanical harvesting layer. And the one on the right displays the multimode pressure signal response and sensing including the top dynamic signal activated by nanogenerators and the bottom static signal excited by piezoresistive or piezocapacitive sensors.

multimode pressure signals. It is ideal to make full use of the energies around the human body, such as solar energy, mechanical energy, temperature gradient, and so on. For instance, a 3D power fabric with multiple energy combination is conceptually presented (left side in Figure 15), which consists of top photovoltaic fibers, middle electrochemical storage fibers, and bottom electromechanical conversion fibers, in which the solar and mechanical energies are harvested and simultaneously stored with the purpose of achieving appreciable, continuous and stable power supply. Human skin can perceive tactile stimuli through cutaneous mechanoreceptors, which inspires us to pursue an artificial skin including fast adaptive and slow adaptive receptors that can respond sensitively and selectively to static and dynamic pressure signals. The integration advantage of 3D fabric structures makes it possible to seamlessly combine the dynamic pressure response ability of the triboelectric or piezoelectric effect with the quasi-static pressure sensing ability of the resistance or capacitance effect. In this case, a dual-mode 3D fabric pressure sensor is designed with the triboelectric or piezoelectric fibers as the upper layer and the resistive or capacitive fibers as the lower layer (right side in Figure 15). When the external load approaches the initial contact, the upper layer will first induce electrostatic charge, which can respond to the tactile range from the proximity to contact, while the lower layer is able to well reflect the small pressure variations from contact to the maximum compressive strain. Therefore, the dual-mode 3D fabric pressure sensor is capable of detecting static and dynamic pressure signals over a wide range. Although no specific research work has been reported, the two examples fully demonstrate the potential advantages of 3D fabric structures in multifunctional integration.

Based on their respective structural characteristics and performance advantages, each 3D fabric TENGs has its own suitable application scenarios. In the process of moving toward the real practical stage, energy and sensing textiles with 3D fabric structures also face many challenges. First of all, in terms of structural design and preparation process, 3D fabrics are much more complicated or difficult to be fabricated than common 2D fabrics. Although 3D fabric forming technology is quite mature in the textile industry, it is still a huge challenge to realize the scalable manufacturing of 3D electronic textiles, considering the integration of a large number of electronic components. Secondly, reasonable circuit design is also crucial for 3D integrated electronic textiles, which require a variety of complex electronic components to be connected in an orderly and reliable manner without causing any wearing burden. Thirdly, the long-term working stability is also greatly challenged due to the increased weak links in the 3D fabric system that the breakdown of one unit will lead to the failure of the whole device, which increases the difficulty of repair or replacement. In particular, good chemical endurance is essential for the long-term operation of 3D electronic textiles, which represents the ability to resist the erosion of various media, including acid, alkali, organic solvent, detergent and other household chemicals. When the surface of textile materials is polluted or working in high humidity/high temperature environment, the charge transfer on the surface of friction layer will be inhibited to a certain extent, so as to reduce the amount of charge transfer and reduce the effective electric output. Surface packaging is one of the effective strategies to avoid chemical damage and maintain good chemical endurance of electronic textiles. Fourthly, in the process of textile preparation, it is inevitable to add a variety of dyes and additives, which will more or less contain chemicals that are harmful to human body. In addition, considering that textile or clothing for wearing needs to be in constant contact

with human skin, some harmful substances or skin sensitive components will contact with the skin, causing skin symptoms, such as itching, inflammation, microbial breeding, and other epidermal symptoms, and even entering the human body to damage tissues and organs. Different from the methods usually used to enhance the electrical output of textile TENGs by adding charge trapping elements into polymer or surface modification of polymer, 3D fabric structural design improves the overall output through the structural extension effect in the thickness direction, which can maintain the original bio-safety of polymer and avoid the safety issues caused by the addition of external elements. Last but not the least, the overall thickness of 3D fabrics will increase to a certain extent, which may lose the original style of fabrics, including flexibility, sense of weight bearing, air permeability, thermal and moisture comfort, and so on. Taking air permeability as an example, the transmission of gas in fabrics is mainly through the gap between fibers. If the gas is blocked by fibers, it will be diffused to the surrounding gap channel. Compared with 2D textile TENGs, the air travel path is longer and the number of blocking fibers in the air flow channel is more in the 3D textile TENGs, which is bound to reduce the overall air permeability. Due to the existence of fiber gap, there are many air transmission channels in the 3D textile TENGs, which endows them with good air permeability. In addition, its air permeability depends on many factors, including fiber size, arrangement spacing, interleaving mode, number of stacking layers, and so on.

No matter how big the challenges are, there is no doubt that these potential difficulties will be overcome one by one with the progress of related science and technology. It is hoped that the timely and comprehensive summary and discussion of advanced 3D fabric TENGs will provide a unique strategy for pursuing high-performance energy and sensing textiles with either high power output or high pressure sensitivity.

Acknowledgements

K.D. and X.P. contributed equally to this work. The authors are grateful for the support received from the National Key R & D Project from Minister of Science and Technology (Grant No. 2021YFA1201601), National Natural Science Foundation of China (Grant No. 22109012), Natural Science Foundation of the Beijing Municipality (Grant No. 2212052), and the Fundamental Research Funds for the Central Universities (Grant No. E1E46805).

Conflict of Interest

The authors declare no conflict of interest.

Keywords

3D fabrics, energy and sensing textiles, power output, pressure sensitivity, triboelectric nanogenerators

Received: November 18, 2021
Revised: January 25, 2022
Published online:

[1] K. Dong, X. Peng, Z. L. Wang, *Adv. Mater.* **2020**, *32*, 1902549.
[2] J. M. Donelan, Q. Li, V. Naing, J. A. Hoffer, D. J. Weber, A. D. Kuo, *Science* **2008**, *319*, 807.
[3] T. Ding, K. H. Chan, Y. Zhou, X.-Q. Wang, Y. Cheng, T. Li, G. W. Ho, *Nat. Commun.* **2020**, *11*, 6006.
[4] J. He, C. Lu, H. Jiang, F. Han, X. Shi, J. Wu, L. Wang, T. Chen, J. Wang, Y. Zhang, H. Yang, G. Zhang, X. Sun, B. Wang, P. Chen, Y. Wang, Y. Xia, H. Peng, *Nature* **2021**, *597*, 57.
[5] E. Pomerantseva, F. Bonaccorso, X. Feng, Y. Cui, Y. Gogotsi, *Science* **2019**, *366*, eaan8285.
[6] W. Yang, W. Gong, W. Gu, Z. Liu, C. Hou, Y. Li, Q. Zhang, H. Wang, *Adv. Mater.* **2021**, *33*, 2104681.
[7] Z. Hu, Y. Li, J.-a. Lv, *Nat. Commun.* **2021**, *12*, 3211.
[8] Y. Luo, Y. Li, P. Sharma, W. Shou, K. Wu, M. Foshey, B. Li, T. Palacios, A. Torralba, W. Matusik, *Nat. Electron.* **2021**, *4*, 193.
[9] A. Hajiaghajani, A. H. Afandizadeh Zargari, M. Dautta, A. Jimenez, F. Kurdahi, P. Tseng, *Nat. Electron.* **2021**, *4*, 808.
[10] Y. Yang, X. Wei, N. Zhang, J. Zheng, X. Chen, Q. Wen, X. Luo, C.-Y. Lee, X. Liu, X. Zhang, J. Chen, C. Tao, W. Zhang, X. Fan, *Nat. Commun.* **2021**, *12*, 4876.
[11] Y. Zhou, B. Braverman, A. Fyffe, R. Zhang, J. Zhao, A. E. Willner, Z. Shi, R. W. Boyd, *Nat. Commun.* **2021**, *12*, 1866.
[12] X. Shi, Y. Zuo, P. Zhai, J. Shen, Y. Yang, Z. Gao, M. Liao, J. Wu, J. Wang, X. Xu, Q. Tong, B. Zhang, B. Wang, X. Sun, L. Zhang, Q. Pei, D. Jin, P. Chen, H. Peng, *Nature* **2021**, *591*, 240.
[13] Q. Jiang, H. Yuan, K. Dong, J.-H. Lin, L. Wu, Y. Tang, *Mater. Des.* **2021**, *205*, 109761.
[14] H. Fan, K. Li, X. Liu, K. Xu, Y. Su, C. Hou, Q. Zhang, Y. Li, H. Wang, *ACS Appl. Mater. Interfaces* **2020**, *12*, 28451.
[15] L. Wang, F. Zhang, Y. Liu, J. Leng, *Adv. Fiber Mater.* **2022**, *4*, 5.
[16] S. Zeng, S. Pian, M. Su, Z. Wang, M. Wu, X. Liu, M. Chen, Y. Xiang, J. Wu, M. Zhang, Q. Cen, Y. Tang, X. Zhou, Z. Huang, R. Wang, A. Tunuhe, X. Sun, Z. Xia, M. Tian, M. Chen, X. Ma, L. Yang, J. Zhou, H. Zhou, Q. Yang, X. Li, Y. Ma, G. Tao, *Science* **2021**, *373*, 692.
[17] Q. Gao, T. Lauster, B. A. F. Kopera, M. Retsch, S. Agarwal, A. Greiner, *Adv. Funct. Mater.* **2021**, *32*, 2108808.
[18] a) W. J. Lee, E. Paineau, D. B. Anthony, Y. Gao, H. S. Leese, S. Rouzière, P. Launois, M. S. P. Schaffer, *ACS Nano* **2020**, *14*, 5570; b) C. Ning, R. Cheng, Y. Jiang, F. Sheng, J. Yi, S. Shen, Y. Zhang, X. Peng, K. Dong, Z. L. Wang, *ACS Nano* **2022**, *16*, 2811.
[19] Y. Wang, L. Li, D. Hofmann, J. E. Andrade, C. Daraio, *Nature* **2021**, *596*, 238.
[20] X. Yu, Y. Li, X. Wang, Y. Si, J. Yu, B. Ding, *ACS Appl. Mater. Interfaces* **2020**, *12*, 32078.
[21] X. Yu, Z. Xie, Y. Yu, J. Lee, A. Vazquez-Guardado, H. Luan, J. Ruban, X. Ning, A. Akhtar, D. Li, B. Ji, Y. Liu, R. Sun, J. Cao, Q. Huo, Y. Zhong, C. Lee, S. Kim, P. Gutruf, C. Zhang, Y. Xue, Q. Guo, A. Chempakasseril, P. Tian, W. Lu, J. Jeong, Y. Yu, J. Cornman, C. Tan, B. Kim, et al., *Nature* **2019**, *575*, 473.
[22] J. Chen, Y. Huang, N. Zhang, H. Zou, R. Liu, C. Tao, X. Fan, Z. L. Wang, *Nat. Energy* **2016**, *1*, 16138.
[23] X. Tian, P. M. Lee, Y. J. Tan, T. L. Y. Wu, H. Yao, M. Zhang, Z. Li, K. A. Ng, B. C. K. Tee, J. S. Ho, *Nat. Electron.* **2019**, *2*, 243.
[24] W. Fan, Q. He, K. Meng, X. Tan, Z. Zhou, G. Zhang, J. Yang, Z. L. Wang, *Sci. Adv.* **2020**, *6*, eaay2840.
[25] a) L. Lao, D. Shou, Y. S. Wu, J. T. Fan, *Sci. Adv.* **2020**, *6*, eaaz0013; b) Y. Peng, W. Li, B. Liu, W. Jin, J. Schaadt, J. Tang, G. Zhou, G. Wang, J. Zhou, C. Zhang, Y. Zhu, W. Huang, T. Wu, K. E. Goodson, C. Dames, R. Prasher, S. Fan, Y. Cui, *Nat. Commun.* **2021**, *12*, 6122.
[26] J. Zhao, W. Zhu, X. Wang, L. Liu, J. Yu, B. Ding, *ACS Nano* **2020**, *14*, 1045.
[27] T. Gao, Z. Yang, C. Chen, Y. Li, K. Fu, J. Dai, E. M. Hitz, H. Xie, B. Liu, J. Song, B. Yang, L. Hu, *ACS Nano* **2017**, *11*, 11513.

[28] L.-X. Liu, W. Chen, H.-B. Zhang, Q.-W. Wang, F. Guan, Z.-Z. Yu, *Adv. Funct. Mater.* **2019**, *29*, 1905197.
[29] M.-W. Han, S.-H. Ahn, *Adv. Mater.* **2017**, *29*, 1606580.
[30] C. S. Haines, M. D. Lima, N. Li, G. M. Spinks, J. Foroughi, J. D. W. Madden, S. H. Kim, S. Fang, M. Jung de Andrade, F. Göktepe, Ö. Göktepe, S. M. Mirvakili, S. Naficy, X. Lepró, J. Oh, M. E. Kozlov, S. J. Kim, X. Xu, B. J. Swedlove, G. G. Wallace, R. H. Baughman, *Science* **2014**, *343*, 868.
[31] M. Stoppa, A. Chiolerio, *Sensors* **2014**, *14*, 11957.
[32] K. Cherenack, L. van Pieterson, *J. Appl. Phys.* **2012**, *112*, 091301.
[33] C. Hertleer, L. Van Langenhove, A. Schwarz, *Intelligent Textiles and Clothing for Ballistic and NBC Protection*, Springer, Dordrecht, The Netherlands **2012**, p. 119.
[34] M. Chen, Y. Jiang, N. Guizani, J. Zhou, G. Tao, J. Yin, K. Hwang, *IEEE Netw.* **2020**, *34*, 156.
[35] H. Wang, Y. Zhang, X. Liang, Y. Zhang, *ACS Nano* **2021**, *15*, 12497.
[36] S. Zhai, H. E. Karahan, C. Wang, Z. Pei, L. Wei, Y. Chen, *Adv. Mater.* **2020**, *32*, 1902387.
[37] D. Yu, Q. Qian, L. Wei, W. Jiang, K. Goh, J. Wei, J. Zhang, Y. Chen, *Chem. Soc. Rev.* **2015**, *44*, 647.
[38] F. Mo, G. Liang, Z. Huang, H. Li, D. Wang, C. Zhi, *Adv. Mater.* **2019**, *32*, 1902151.
[39] J. Zhou, J. Cheng, B. Wang, H. Peng, J. Lu, *Energy Environ. Sci.* **2020**, *13*, 1933.
[40] D. G. Mackanic, T. H. Chang, Z. Huang, Y. Cui, Z. Bao, *Chem. Soc. Rev.* **2020**, *49*, 4466.
[41] H. Sun, Y. Zhang, J. Zhang, X. Sun, H. Peng, *Nat. Rev. Mater.* **2017**, *2*, 17023.
[42] Y. Zhou, C. H. Wang, W. Lu, L. Dai, *Adv. Mater.* **2020**, *32*, 1902779.
[43] U. Gulzar, S. Goriparti, E. Miele, T. Li, G. Maidecchi, A. Toma, F. De Angelis, C. Capiglia, R. P. Zaccaria, *J. Mater. Chem. A* **2016**, *4*, 16771.
[44] M. Tebyetekerwa, I. Marriam, Z. Xu, S. Yang, H. Zhang, F. Zabihi, R. Jose, S. Peng, M. Zhu, S. Ramakrishna, *Energy Environ. Sci.* **2019**, *12*, 2148.
[45] L. Yin, K. N. Kim, A. Trifonov, T. Podhajny, J. Wang, *Energy Environ. Sci.* **2022**, *15*, 82.
[46] Y. Bai, H. Jantunen, J. Juuti, *Adv. Mater.* **2018**, *30*, 1707271.
[47] H. Ryu, H.-J. Yoon, S.-W. Kim, *Adv. Mater.* **2019**, *31*, 1802898.
[48] X. Pu, W. Song, M. Liu, C. Sun, C. Du, C. Jiang, X. Huang, D. Zou, W. Hu, Z. L. Wang, *Adv. Energy Mater.* **2016**, *6*, 1601048.
[49] M. Hatamvand, E. Kamrani, M. Lira-Cantú, M. Madsen, Y. Zhan, *Nano Energy* **2020**, *71*, 104609.
[50] L. Wang, K. Zhang, *Energy Environ. Mater.* **2020**, *3*, 67.
[51] L. S. Zhang, B. Yang, S. P. Lin, T. Hua, X. M. Tao, *Nano Energy* **2020**, *76*, 105117.
[52] A. J. Bandodkar, J.-M. You, N.-H. Kim, Y. Gu, R. Kumar, A. M. V. Mohan, J. Kurniawan, S. Imani, T. Nakagawa, B. Parish, M. Parthasarathy, P. P. Mercier, S. Xu, J. Wang, *Energy Environ. Sci.* **2017**, *10*, 1581.
[53] S. Yin, Z. Jin, T. Miyake, *Biosens. Bioelectron.* **2019**, *141*, 111471.
[54] S. Kwon, Y. H. Hwang, M. Nam, H. Chae, H. S. Lee, Y. Jeon, S. Lee, C. Y. Kim, S. Choi, E. G. Jeong, K. C. Choi, *Adv. Mater.* **2020**, *32*, 1903488.
[55] C. Wu, A. C. Wang, W. Ding, H. Guo, Z. L. Wang, *Adv. Energy Mater.* **2019**, *9*, 1802906.
[56] Z. L. Wang, *Mater. Today* **2017**, *20*, 74.
[57] Z. L. Wang, *Rep. Prog. Phys.* **2021**, *84*, 096502.
[58] K. Dong, Y.-C. Wang, J. Deng, Y. Dai, S. L. Zhang, H. Zou, B. Gu, B. Sun, Z. L. Wang, *ACS Nano* **2017**, *11*, 9490.
[59] Y. Wang, Y. Yang, Z. L. Wang, *npj Flexible Electron.* **2017**, *1*, 10.
[60] K. Dong, X. Peng, J. An, A. C. Wang, J. Luo, B. Sun, J. Wang, Z. L. Wang, *Nat. Commun.* **2020**, *11*, 2868.
[61] C. Ye, K. Dong, J. An, J. Yi, X. Peng, C. Ning, Z. L. Wang, *ACS Energy Lett.* **2021**, *6*, 1443.
[62] K. Dong, Z. Wu, J. Deng, A. C. Wang, H. Zou, C. Chen, D. Hu, B. Gu, B. Sun, Z. L. Wang, *Adv. Mater.* **2018**, *30*, 1804944.
[63] Y. Jiang, K. Dong, X. Li, J. An, D. Wu, X. Peng, J. Yi, C. Ning, R. Cheng, P. Yu, Z. L. Wang, *Adv. Funct. Mater.* **2020**, 2005584.
[64] Z. Wu, T. Cheng, Z. L. Wang, *Sensors* **2020**, *20*, 2925.
[65] X. Peng, K. Dong, Z. Wu, J. Wang, Z. L. Wang, *J. Mater. Sci.* **2021**, *56*, 16765.
[66] X. Peng, K. Dong, C. Ye, Y. Jiang, S. Zhai, R. Cheng, D. Liu, X. Gao, J. Wang, Z. L. Wang, *Sci. Adv.* **2020**, *6*, eaba9624.
[67] K. Meng, S. Zhao, Y. Zhou, Y. Wu, S. Zhang, Q. He, X. Wang, Z. Zhou, W. Fan, X. Tan, J. Yang, J. Chen, *Matter* **2020**, *2*, 896.
[68] K. Dong, J. Deng, W. Ding, A. C. Wang, P. Wang, C. Cheng, Y.-C. Wang, L. Jin, B. Gu, B. Sun, Z. L. Wang, *Adv. Energy Mater.* **2018**, *8*, 1801114.
[69] C. Ning, K. Dong, R. Cheng, J. Yi, C. Ye, X. Peng, F. Sheng, Y. Jiang, Z. L. Wang, *Adv. Funct. Mater.* **2020**, *31*, 2006679.
[70] Q. Shi, Z. Zhang, T. He, Z. Sun, B. Wang, Y. Feng, X. Shan, B. Salam, C. Lee, *Nat. Commun.* **2020**, *11*, 4609.
[71] Z. Zhang, T. He, M. Zhu, Z. Sun, Q. Shi, J. Zhu, B. Dong, M. R. Yuce, C. Lee, *npj Flex. Electron.* **2020**, *4*, 29.
[72] K. Dong, Y. Hu, J. Yang, S. W. Kim, W. Hu, Z. L. Wang, *MRS Bull.* **2021**, *46*, 512.
[73] K. Dong, Z. L. Wang, *J. Semicond.* **2021**, *42*, 101601.
[74] L. Jin, X. Xiao, W. Deng, A. Nashalian, J. Chen, *Nano Lett.* **2020**, *20*, 6404.
[75] T. Jing, B. Xu, Y. Yang, C. Jiang, M. Wu, *Nano Energy* **2020**, *78*, 105374.
[76] J. Wang, S. Li, F. Yi, Y. Zi, J. Lin, X. Wang, Y. Xu, Z. L. Wang, *Nat. Commun.* **2016**, *7*, 12744.
[77] P. Cheng, H. Guo, Z. Wen, C. Zhang, X. Yin, X. Li, D. Liu, W. Song, X. Sun, J. Wang, *Nano Energy* **2018**, *57*, 432.
[78] J. Chun, B. U. Ye, J. W. Lee, D. Choi, C. Y. Kang, S. W. Kim, Z. L. Wang, J. M. Baik, *Nat. Commun.* **2016**, *7*, 12985.
[79] D. Liu, X. Yin, H. Guo, L. Zhou, X. Li, C. Zhang, J. Wang, Z. L. Wang, *Sci. Adv.* **2019**, *5*, aav6437.
[80] H. Wang, L. Xu, Y. Bai, Z. L. Wang, *Nat. Commun.* **2020**, *11*, 4203.
[81] L. Xu, T. Z. Bu, X. D. Yang, C. Zhang, Z. L. Wang, *Nano Energy* **2018**, *49*, 625.
[82] C. Fang, T. Tong, T. Bu, Y. Cao, C. Zhang, *Adv. Intell. Syst.* **2020**, *2*, 2070020.
[83] W. Liu, Z. Wang, G. Wang, Q. Zeng, W. He, L. Liu, X. Wang, Y. Xi, H. Guo, C. Hu, Z. L. Wang, *Nat. Commun.* **2020**, *11*, 1883.
[84] J. Wang, C. Wu, Y. Dai, Z. Zhao, A. Wang, T. Zhang, Z. L. Wang, *Nat. Commun.* **2017**, *8*, 88.
[85] J. Lee, B. L. Zambrano, J. Woo, K. Yoon, T. Lee, *Adv. Mater.* **2019**, *32*, 1902532.
[86] L. Huang, S. Lin, Z. Xu, H. Zhou, J. Zhou, *Adv. Mater.* **2019**, *32*, 1902034.
[87] Y.-H. Zhu, X.-Y. Yang, T. Liu, X.-B. Zhang, *Adv. Mater.* **2020**, *32*, 1901961.
[88] K. Bilisik, N. S. Karaduman, N. E. Bilisik, in *Non-Woven Fabrics* (Ed: H.-Y. Jeon), IntechOpen, London, UK, **2016**, Ch. 4.
[89] N. Ishmael, A. Fernando, S. Andrew, L. W. Taylor, *Res. J. Tex. Apparel* **2017**, *21*, 342.
[90] K. Bilisik, *Tex. Res. J.* **2012**, *82*, 725.
[91] K. Dong, K. Liu, L. Pan, B. Gu, B. Sun, *Compos. Struct.* **2016**, *154*, 319.
[92] P. G. Unal, in *Woven Fabrics* (Ed: H.-Y. Jeon), IntechOpen, London, UK, **2012**, pp. 91–120.
[93] A. Levitt, D. Hegh, P. Phillips, S. Uzun, G. Dion, *Mater. Today* **2020**, *34*, 17.
[94] Y. Zhang, H. Hu, Y. Kyosev, Y. Liu, *Compos. Struct.* **2019**, *236*, 111846.
[95] K. Dong, J. Zhang, L. Jin, B. Gu, B. Sun, *Compos. Struct.* **2016**, *143*, 9.

[96] L. B. Venu, E. Shim, N. Anantharamaiah, B. Pourdeyhimi, *Microsc. Microanal.* **2012**, *18*, 1368.
[97] K. M. Raghvendra, L. Sravanthi, *Mod. Chem. Appl.* **2017**, *5*, 2.
[98] M. K. Joshi, R. M. Shrestha, H. R. Pant, in *Generation, Development and Modifications of Natural Fibers* (Eds: M. Abbass, H.-Y. Jeon), IntechOpen, London, UK **2020**, Ch. 6.
[99] H. Sahasrabudhe, S. Bose, A. Bandyopadhyay, *Advances in Laser Materials Processing*, Woodhead Publishing, Cambridge, UK **2018**, p. 507.
[100] K. Chatterjee, T. K. Ghosh, *Adv. Mater.* **2020**, *32*, 1902086.
[101] S. Pyo, J. Lee, W. Kim, E. Jo, J. Kim, *Adv. Funct. Mater.* **2019**, *29*, 1902484.
[102] F. R. Fan, L. Lin, G. Zhu, W. Wu, R. Zhang, Z. L. Wang, *Nano Lett.* **2012**, *12*, 3109.
[103] Z. L. Wang, *Faraday Discuss.* **2014**, *176*, 447.
[104] Z. Lin, J. Yang, X. Li, Y. Wu, W. Wei, J. Liu, J. Chen, J. Yang, *Adv. Funct. Mater.* **2018**, *28*, 1704112.
[105] Z. Li, J. Shen, I. Abdalla, J. Yu, B. Ding, *Nano Energy* **2017**, *36*, 341.
[106] H. Guo, X. Pu, J. Chen, Y. Meng, M.-H. Yeh, G. Liu, Q. Tang, B. Chen, D. Liu, S. Qi, C. Wu, C. Hu, J. Wang, Z. L. Wang, *Sci. Rob.* **2018**, *3*, eaat2516.
[107] Z. Yan, L. Wang, Y. Xia, R. Qiu, W. Liu, M. Wu, Y. Zhu, S. Zhu, C. Jia, M. Zhu, R. Cao, Z. Li, X. Wang, *Adv. Funct. Mater.* **2021**, *31*, 2100709.
[108] J. Chen, X. Pu, H. Guo, Q. Tang, L. Feng, X. Wang, C. Hu, *Nano Energy* **2018**, *43*, 253.
[109] J. J. Kim, Y. Wang, H. Wang, S. Lee, T. Yokota, T. Someya, *Adv. Funct. Mater.* **2021**, *31*, 2009602.
[110] F. Sheng, J. Yi, S. Shen, R. Cheng, C. Ning, L. Ma, X. Peng, W. Deng, K. Dong, Z. L. Wang, *ACS Appl. Mater. Interfaces* **2021**, *13*, 44868.
[111] G. Chen, C. Au, J. Chen, *Trends Biotechnol.* **2021**, *39*, 1078.
[112] X. Peng, K. Dong, C. Ning, R. Cheng, J. Yi, Y. Zhang, F. Sheng, Z. Wu, Z. L. Wang, *Adv. Funct. Mater.* **2021**, *31*, 2103559.
[113] Y.-C. Lai, J. Deng, R. Liu, Y.-C. Hsiao, S. L. Zhang, W. Peng, H.-M. Wu, X. Wang, Z. L. Wang, *Adv. Mater.* **2018**, *30*, 1801114.
[114] D. Jiang, H. Ouyang, B. Shi, Y. Zou, P. Tan, X. Qu, S. Chao, Y. Xi, C. Zhao, Y. Fan, Z. Li, *InfoMat* **2020**, *2*, 1191.
[115] M. Zhu, Z. Sun, T. Chen, C. Lee, *Nat. Commun.* **2021**, *12*, 2692.
[116] X. Gang, Z. H. Guo, Z. Cong, J. Wang, C. Chang, C. Pan, X. Pu, Z. L. Wang, *ACS Appl. Mater. Interfaces* **2021**, *13*, 20145.
[117] Z. L. Wang, P. Chen, *Physics* **2021**, *50*, 649.
[118] Z. L. Wang, T. Jiang, L. Xu, *Nano Energy* **2017**, *39*, 9.
[119] C. Xu, Y. Zi, A. C. Wang, H. Zou, Y. Dai, X. He, P. Wang, Y. C. Wang, P. Feng, D. Li, Z. L. Wang, *Adv. Mater.* **2018**, *30*, 1706790.
[120] C. Xu, A. C. Wang, H. Zou, B. Zhang, C. Zhang, Y. Zi, L. Pan, P. Wang, P. Feng, Z. Lin, Z. L. Wang, *Adv. Mater.* **2018**, *30*, 1803968.
[121] S. Lin, X. Chen, Z. L. Wang, *Chem. Rev.* **2022**, *122*, 5209.
[122] P. Cheng, H. Guo, Z. Wen, C. Zhang, X. Yin, X. Li, D. Liu, W. Song, X. Sun, J. Wang, Z. L. Wang, *Nano Energy* **2019**, *57*, 432.
[123] Y. Park, Y. E. Shin, J. Park, Y. Lee, M. P. Kim, Y. R. Kim, S. Na, S. K. Ghosh, H. Ko, *ACS Nano* **2020**, *14*, 7101.
[124] H. Jiang, H. Lei, Z. Wen, J. Shi, D. Bao, C. Chen, J. Jiang, Q. Guan, X. Sun, S.-T. Lee, *Nano Energy* **2020**, *75*, 105011.
[125] H. Zou, Y. Zhang, L. Guo, P. Wang, X. He, G. Dai, H. Zheng, C. Chen, A. C. Wang, C. Xu, Z. L. Wang, *Nat. Commun.* **2019**, *10*, 1427.
[126] H. Zou, L. Guo, H. Xue, Y. Zhang, Z. L. Wang, *Nat. Commun.* **2020**, *11*, 2093.
[127] M. Seol, S. Kim, Y. Cho, K.-E. Byun, H. Kim, J. Kim, S. K. Kim, S.-W. Kim, H.-J. Shin, S. Park, *Adv. Mater.* **2018**, *30*, 1801210.
[128] P.-Y. Feng, Z. Xia, B. Sun, X. Jing, H. Li, X. Tao, H.-Y. Mi, Y. Liu, *ACS Appl. Mater. Interfaces* **2021**, *13*, 16916.
[129] S. Li, Y. Fan, H. Chen, J. Nie, Y. Liang, X. Tao, J. Zhang, X. Chen, E. Fu, Z. L. Wang, *Energy Environ. Sci.* **2020**, *13*, 896.
[130] Y. Fan, S. Li, X. Tao, Y. Wang, Z. Liu, H. Chen, Z. Wu, J. Zhang, F. Ren, X. Chen, E. Fu, *Nano Energy* **2021**, *90*, 106574.
[131] Z. Zhao, L. Zhou, S. Li, D. Liu, Y. Li, Y. Gao, Y. Liu, Y. Dai, J. Wang, Z. L. Wang, *Nat. Commun.* **2021**, *12*, 4686.
[132] Z. Zhao, Y. Dai, D. Liu, L. Zhou, S. Li, Z. L. Wang, J. Wang, *Nat. Commun.* **2020**, *11*, 6186.
[133] R. Cheng, K. Dong, P. Chen, C. Ning, X. Peng, Y. Zhang, D. Liu, Z. L. Wang, *Energy Environ. Sci.* **2021**, *14*, 2460.
[134] K. Dong, J. Deng, Y. Zi, Y.-C. Wang, C. Xu, H. Zou, W. Ding, Y. Dai, B. Gu, B. Sun, Z. L. Wang, *Adv. Mater.* **2017**, *29*, 1702648.
[135] E. He, Y. Sun, X. Wang, H. Chen, B. Sun, B. Gu, W. Zhang, *Composites, Part B* **2020**, *200*, 108244.
[136] L. Ma, R. Wu, S. Liu, A. Patil, H. Gong, J. Yi, F. Sheng, Y. Zhang, J. Wang, J. Wang, W. Guo, Z. L. Wang, *Adv. Mater.* **2020**, *32*, 2003897.
[137] C. Chen, L. Chen, Z. Wu, H. Guo, W. Yu, Z. Du, Z. L. Wang, *Mater. Today* **2020**, *32*, 84.
[138] S. S. Kwak, H. Kim, W. Seung, J. Kim, R. Hinchet, S. W. Kim, *ACS Nano* **2017**, *11*, 10733.
[139] L. Liu, J. Pan, P. Chen, J. Zhang, X. Yu, X. Ding, B. Wang, X. Sun, H. Peng, *J. Mater. Chem. A* **2016**, *4*, 6077.
[140] D.-H. Kwon, J.-H. Kwon, J. Jeong, Y. Lee, S. Biswas, D.-W. Lee, S. Lee, J.-H. Bae, H. Kim, *Electronics* **2021**, *10*, 937.
[141] J.-H. Kwon, J. Jeong, Y. Lee, S. Biswas, J.-K. Park, S. Lee, D.-W. Lee, S. Lee, J.-H. Bae, H. Kim, *Macromol. Res.* **2021**, *29*, 443.
[142] M. Zhu, Y. Huang, W. S. Ng, J. Liu, Z. Wang, Z. Wang, H. Hu, C. Zhi, *Nano Energy* **2016**, *27*, 439.
[143] Q. Wang, X. Peng, Y. Zu, L. Jiang, K. Dong, *J. Phys. D: Appl. Phys.* **2021**, *54*, 424006.
[144] J. Gong, B. Xu, X. Guan, Y. Chen, S. Li, J. Feng, *Nano Energy* **2019**, *58*, 365.
[145] Z. Wang, Z. Ruan, W. S. Ng, H. Li, Z. Tang, Z. Liu, Y. Wang, H. Hu, C. Zhi, *Small Methods* **2018**, *2*, 1800150.
[146] X. Peng, K. Dong, C. Ye, Y. Jiang, Z. L. Wang, *Sci. Adv.* **2020**, *6*, eaba9624.
[147] Y. Jiang, K. Dong, J. An, F. Liang, J. Yi, X. Peng, C. Ning, C. Ye, Z. L. Wang, *ACS Appl. Mater. Interfaces* **2021**, *13*, 11205.
[148] Z. Li, M. Zhu, J. Shen, Q. Qiu, B. Ding, *Adv. Funct. Mater.* **2020**, *30*, 1908411.
[149] W. Yang, W. Gong, C. Hou, Y. Su, Y. Guo, W. Zhang, Y. Li, Q. Zhang, H. Wang, *Nat. Commun.* **2019**, *10*, 5541.
[150] W. Gong, X. Wang, W. Yang, J. Zhou, X. Han, M. D. Dickey, Y. Su, C. Hou, Y. Li, Q. Zhang, H. Wang, *Adv. Mater.* **2021**, *33*, 2007352.
[151] H. He, J. Guo, B. Illés, A. Géczy, B. Istók, V. Hliva, D. Török, J. G. Kovács, I. Harmati, K. Molnár, *Nano Energy* **2021**, *89*, 106418.
[152] H. Wang, H. Sakamoto, H. Asai, J.-H. Zhang, T. Meboso, Y. Uchiyama, E. Kobayashi, E. Takamura, S.-i. Suye, *Nano Energy* **2021**, *90*, 106515.
[153] X. Zhang, S. Lv, X. Lu, H. Yu, T. Huang, Q. Zhang, M. Zhu, *Nano Energy* **2020**, *75*, 104894.
[154] A. You, X. Zhang, X. Peng, K. Dong, Y. Lu, Q. Zhang, *Macromol. Mater. Eng.* **2021**, *306*, 2100147.
[155] M. A. P. Mahmud, A. Zolfagharian, S. Gharaie, A. Kaynak, S. H. Farjana, A. V. Ellis, J. Chen, A. Z. Kouzani, *Adv. Energy Sustainability Res.* **2021**, *2*, 2000045.
[156] B. Chen, W. Tang, Z. L. Wang, *Mater. Today* **2021**, *50*, 224.
[157] M.-L. Seol, J.-W. Han, D.-I. Moon, K. J. Yoon, C. S. Hwang, M. Meyyappan, *Nano Energy* **2018**, *44*, 82.
[158] Y. Tong, Z. Feng, J. Kim, J. L. Robertson, B. N. Johnson, *Nano Energy* **2020**, *75*, 104973.
[159] M. Zhang, M. Zhao, M. Jian, C. Wang, A. Yu, Z. Yin, X. Liang, H. Wang, K. Xia, X. Liang, J. Zhai, Y. Zhang, *Matter* **2019**, *1*, 168.
[160] C. Qian, L. Li, M. Gao, H. Yang, Z. Cai, B. Chen, Z. Xiang, Z. Zhang, Y. Song, *Nano Energy* **2019**, *63*, 103885.
[161] B. Chen, W. Tang, T. Jiang, L. Zhu, X. Chen, C. He, L. Xu, H. Guo, P. Lin, D. Li, J. Shao, Z. L. Wang, *Nano Energy* **2018**, *45*, 380.

[162] X. X. Zhu, Z. B. Li, X. S. Li, L. Su, X. Y. Wei, S. Y. Kuang, B. W. Su, J. Yang, Z. L. Wang, G. Zhu, *Nano Energy* **2018**, *50*, 497.
[163] Z. L. Wang, J. Chen, L. Lin, *Energy Environ. Sci.* **2015**, *8*, 2250.
[164] T. He, H. Wang, J. Wang, X. Tian, F. Wen, Q. Shi, J. S. Ho, C. Lee, *Adv. Sci.* **2019**, *6*, 1901437.
[165] R. Cheng, K. Dong, L. Liu, C. Ning, P. Chen, X. Peng, D. Liu, Z. L. Wang, *ACS Nano* **2020**, *14*, 15853.
[166] J. Yi, K. Dong, S. Shen, Y. Jiang, X. Peng, C. Ye, Z. L. Wang, *Nano–Micro Lett.* **2021**, *13*, 103.
[167] C. Ye, D. Liu, X. Peng, Y. Jiang, R. Cheng, C. Ning, F. Sheng, Y. Zhang, K. Dong, Z. L. Wang, *ACS Nano* **2021**, *15*, 18172.
[168] J. Xiong, P. Cui, X. Chen, J. Wang, K. Parida, M.-F. Lin, P. S. Lee, *Nat. Commun.* **2018**, *9*, 4280.
[169] X. Pu, L. Li, H. Song, C. Du, Z. Zhao, C. Jiang, G. Cao, W. Hu, Z. L. Wang, *Adv. Mater.* **2015**, *27*, 2472.
[170] A. Yu, X. Pu, R. Wen, M. Liu, T. Zhou, K. Zhang, Y. Zhang, J. Zhai, W. Hu, Z. L. Wang, *ACS Nano* **2017**, *11*, 12764.
[171] M. Lou, I. Abdalla, M. Zhu, X. Wei, J. Yu, Z. Li, B. Ding, *ACS Appl. Mater. Interfaces* **2020**, *12*, 19965.
[172] L. Shuai, Z. H. Guo, P. Zhang, J. Wan, X. Pu, Z. L. Wang, *Nano Energy* **2020**, *78*, 105389.
[173] Q. He, Y. Wu, Z. Feng, W. Fan, Z. Lin, C. Sun, Z. Zhou, K. Meng, W. Wu, J. Yang, *J. Mater. Chem. A* **2019**, *7*, 26804.
[174] X. Guan, B. Xu, M. Wu, T. Jing, Y. Yang, Y. Gao, *Nano Energy* **2021**, *80*, 105549.
[175] Y.-C. Lai, J. Deng, S. Niu, W. Peng, C. Wu, R. Liu, Z. Wen, Z. L. Wang, *Adv. Mater.* **2016**, *28*, 10024.
[176] Y. Wu, S. Kuang, H. Li, H. Wang, R. Yang, Y. Zhai, G. Zhu, Z. L. Wang, *Adv. Mater. Technol.* **2018**, *3*, 1800166.
[177] X. Yin, D. Liu, L. Zhou, X. Li, C. Zhang, P. Cheng, H. Guo, W. Song, J. Wang, Z. L. Wang, *ACS Nano* **2019**, *13*, 698.
[178] R. Lei, Y. Shi, Y. Ding, J. Nie, S. Li, F. Wang, H. Zhai, X. Chen, Z. L. Wang, *Energy Environ. Sci.* **2020**, *13*, 2178.
[179] Z. Wang, W. Liu, W. He, H. Guo, L. Long, Y. Xi, X. Wang, A. Liu, C. Hu, *Joule* **2021**, *5*, 441.
[180] R. Cao, X. Pu, X. Du, W. Yang, J. Wang, H. Guo, S. Zhao, Z. Yuan, C. Zhang, C. Li, *ACS Nano* **2018**, *12*, 5190.
[181] K. Zhou, Y. Zhao, X. Sun, Z. Yuan, G. Zheng, K. Dai, L. Mi, C. Pan, C. Liu, C. Shen, *Nano Energy* **2020**, *70*, 104546.
[182] Y. Jiang, K. Dong, X. Li, J. An, D. Wu, X. Peng, J. Yi, C. Ning, R. Cheng, P. Yu, Z. L. Wang, *Adv. Funct. Mater.* **2021**, *31*, 2005584.
[183] Y.-W. Cai, X.-N. Zhang, G.-G. Wang, G.-Z. Li, D.-Q. Zhao, N. Sun, F. Li, H.-Y. Zhang, J.-C. Han, Y. Yang, *Nano Energy* **2021**, *81*, 105663.
[184] Z. Liu, J. Lyu, D. Fang, X. Zhang, *ACS Nano* **2019**, *13*, 5703.
[185] Y. Chen, Q. Zhang, Y. Zhong, P. Wei, X. Yu, J. Huang, J. Cai, *Adv. Funct. Mater.* **2021**, *31*, 2104368.
[186] L. M. Ericson, H. Fan, H. Peng, V. A. Davis, W. Zhou, J. Sulpizio, Y. Wang, R. Booker, J. Vavro, C. Guthy, A. N. G. Parra-Vasquez, M. J. Kim, S. Ramesh, K. R. Saini, C. Kittrell, G. Lavin, H. Schmidt, W. W. Adams, W. E. Billups, M. Pasquali, W.-F. Hwang, R. H. Hauge, J. E. Fischer, R. E. Smalley, *Science* **2004**, *305*, 1447.
[187] Z. Xu, C. Gao, *Nat. Commun.* **2011**, *2*, 571.
[188] J. Zhang, S. Seyedin, S. Qin, P. A. Lynch, Z. Wang, W. Yang, X. Wang, J. M. Razal, *J. Mater. Chem. A* **2019**, *7*, 6401.
[189] W. Eom, H. Shin, R. B. Ambade, S. H. Lee, K. H. Lee, D. J. Kang, T. H. Han, *Nat. Commun.* **2020**, *11*, 2825.
[190] M. Yao, B. Wu, X. Feng, S. Sun, P. Wu, *Adv. Mater.* **2021**, *33*, 2103755.
[191] Y. Qin, X. Wang, Z. L. Wang, *Nature* **2008**, *451*, 809.
[192] T. Sun, B. Zhou, Q. Zheng, L. Wang, W. Jiang, G. J. Snyder, *Nat. Commun.* **2020**, *11*, 572.
[193] X. Chen, L. Qiu, J. Ren, G. Guan, H. Lin, Z. Zhang, P. Chen, Y. Wang, H. Peng, *Adv. Mater.* **2013**, *25*, 6436.
[194] H. Lin, W. Weng, J. Ren, L. Qiu, Z. Zhang, P. Chen, X. Chen, J. Deng, Y. Wang, H. Peng, *Adv. Mater.* **2014**, *26*, 1217.
[195] J. Lee, S. J. Ihle, G. S. Pellegrino, H. Kim, J. Yea, C.-Y. Jeon, H.-C. Son, C. Jin, D. Eberli, F. Schmid, B. L. Zambrano, A. F. Renz, C. Forró, H. Choi, K.-I. Jang, R. Küng, J. Vörös, *Nat. Electron.* **2021**, *4*, 291.
[196] M. Kanik, S. Orguc, G. Varnavides, J. Kim, T. Benavides, D. Gonzalez, T. Akintilo, C. C. Tasan, P. Chandrakasan Anantha, Y. Fink, P. Anikeeva, *Science* **2019**, *365*, 145.
[197] C. S. Haines, N. Li, G. M. Spinks, A. E. Aliev, J. Di, R. H. Baughman, *Proc. Natl. Acad. Sci. USA* **2016**, *113*, 11709.
[198] Z. Zhang, K. Guo, Y. Li, X. Li, G. Guan, H. Li, Y. Luo, F. Zhao, Q. Zhang, B. Wei, Q. Pei, H. Peng, *Nat. Photonics* **2015**, *9*, 233.
[199] H. Bai, S. Li, J. Barreiros, Y. Tu, R. Pollock Clifford, F. Shepherd Robert, *Science* **2020**, *370*, 848.
[200] C. Jiang, X. Li, Y. Ying, J. Ping, *Nano Energy* **2020**, *74*, 104863.
[201] C. Ning, K. Dong, W. Gao, F. Sheng, R. Cheng, Y. Jiang, J. Yi, C. Ye, X. Peng, Z. L. Wang, *Chem. Eng. J.* **2021**, *420*, 129650.
[202] J. Han, C. Xu, J. Zhang, N. Xu, Y. Xiong, X. Cao, Y. Liang, L. Zheng, J. Sun, J. Zhai, Q. Sun, Z. L. Wang, *ACS Nano* **2021**, *15*, 1597.
[203] D. Zhang, W. Yang, W. Gong, W. Ma, C. Hou, Y. Li, Q. Zhang, H. Wang, *Adv. Mater.* **2021**, *33*, 2100782.
[204] Z. Feng, S. Yang, S. Jia, Y. Zhang, S. Jiang, L. Yu, R. Li, G. Song, A. Wang, T. Martin, L. Zuo, X. Jia, *Nano Energy* **2020**, *74*, 104805.
[205] L. Ma, M. Zhou, R. Wu, A. Patil, H. Gong, S. Zhu, T. Wang, Y. Zhang, S. Shen, K. Dong, L. Yang, J. Wang, W. Guo, Z. L. Wang, *ACS Nano* **2020**, *14*, 4716.
[206] Y.-C. Lai, H.-W. Lu, H.-M. Wu, D. Zhang, J. Yang, J. Ma, M. Shamsi, V. Vallem, M. D. Dickey, *Adv. Energy Mater.* **2021**, *11*, 2100411.
[207] S. Dong, F. Xu, Y. Sheng, Z. Guo, X. Pu, Y. Liu, *Nano Energy* **2020**, *78*, 105327.
[208] W. Wang, A. Yu, X. Liu, Y. Liu, Z. L. Wang, *Nano Energy* **2020**, *71*, 104605.
[209] T. Jing, B. Xu, Y. Yang, *Nano Energy* **2021**, *84*, 105867.
[210] D. Doganay, M. O. Cicek, M. B. Durukan, B. Altuntas, E. Agbahca, S. Coskun, H. E. Unalan, *Nano Energy* **2021**, *89*, 106412.
[211] X. Guan, B. Xu, M. Wu, T. Jing, Y. Gao, *Nano Energy* **2021**, *80*, 105549.
[212] Y. Li, J. Xiong, J. Lv, J. Chen, D. Gao, X. Zhang, P. S. Lee, *Nano Energy* **2020**, *78*, 105358.
[213] M.-F. Lin, J. Xiong, J. Wang, K. Parida, P. S. Lee, *Nano Energy* **2018**, *44*, 248.
[214] X. Tian, T. Hua, *ACS Sustainable Chem. Eng.* **2021**, *9*, 13356.

Kai Dong is an associate professor in the Beijing Institute of Nanoenergy and Nanosystems at the Chinese Academy of Sciences, China. He received his M.S. and Ph.D. degrees in textile science and engineering from Donghua University, China, in 2015 and 2018, respectively. He was a visiting scholar at the school of Materials Science and Engineering of Georgia Institute of Technology, USA, from 2016 to 2018. He joined Donghua University from November 2018 to June 2019 as a faculty member. His main research interests include smart/electronic textiles, fiber/fabric-based piezoelectric and triboelectric nanogenerators, and textile-based self-powered wearable sensors, electronic skins, and soft robotics.

Zhong Lin Wang is the director of the Beijing Institute of Nanoenergy and Nanosystems. He pioneered nanogenerators from fundamental science to technological applications. His research on self-powered nanosystems has inspired the worldwide effort in academia and industry for studying energy for micro-nanosystems. He coined and pioneered the fields of piezotronics and piezophototronics for third-generation semiconductors. He has received the Celsius Lecture Laureate, Uppsala University, Sweden (2020); The Albert Einstein World Award of Science (2019); Diels-Planck Lecture Award (2019); and the ENI Award in Energy Frontiers (2018); Global Nanoenergy Prize, Thomas Router Citation Laureate in Physics (2015).